Development of Laser Sources and Diagnostics for Probing Relativistic Laser-Matter Interaction

Master thesis

Martin Beyer

supervisors:

Prof. Dr. Malte Kaluza

Dr. Yasmina Azamoum

December 9th, 2022

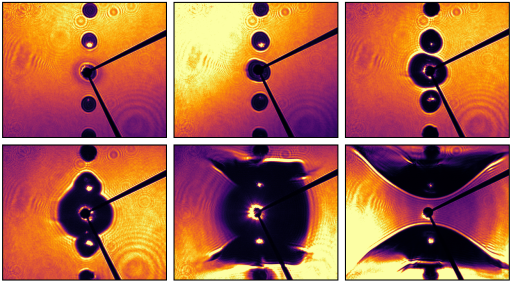

The Dilemma

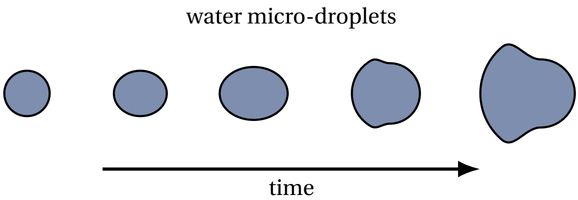

The Dilemma

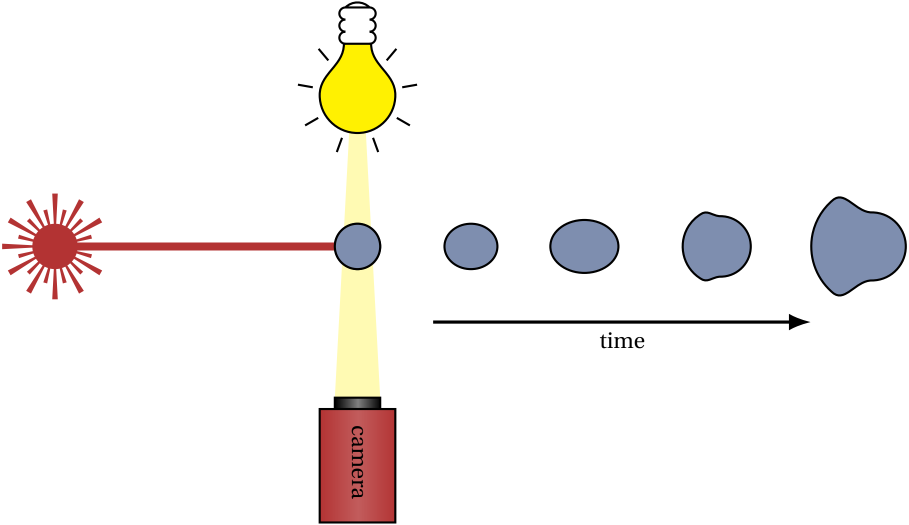

The Dilemma

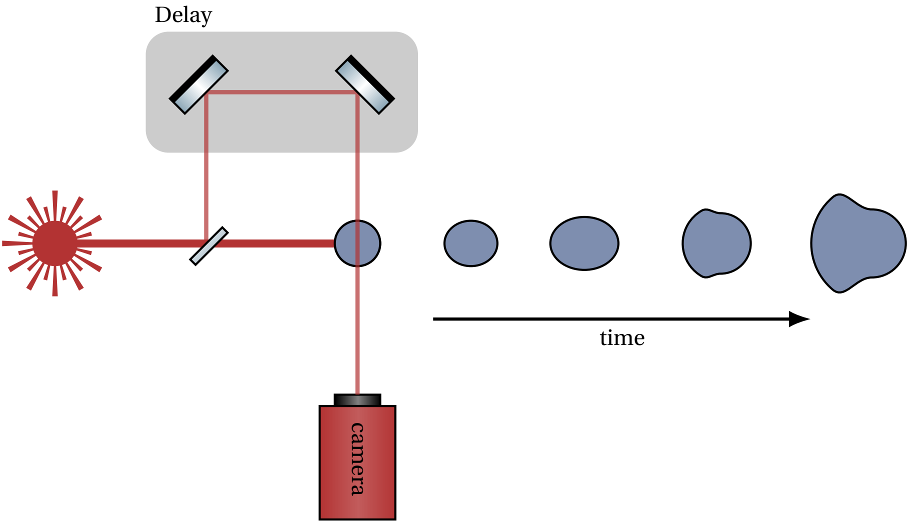

The Dilemma

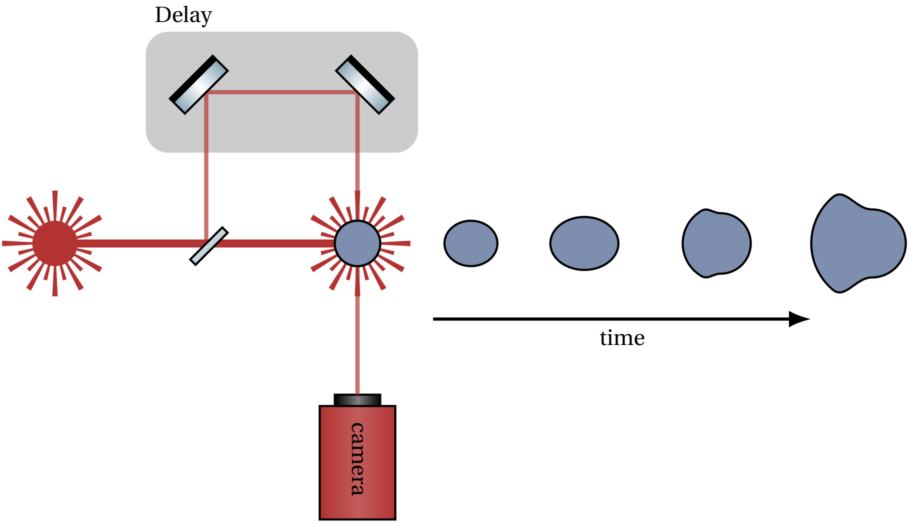

The Dilemma

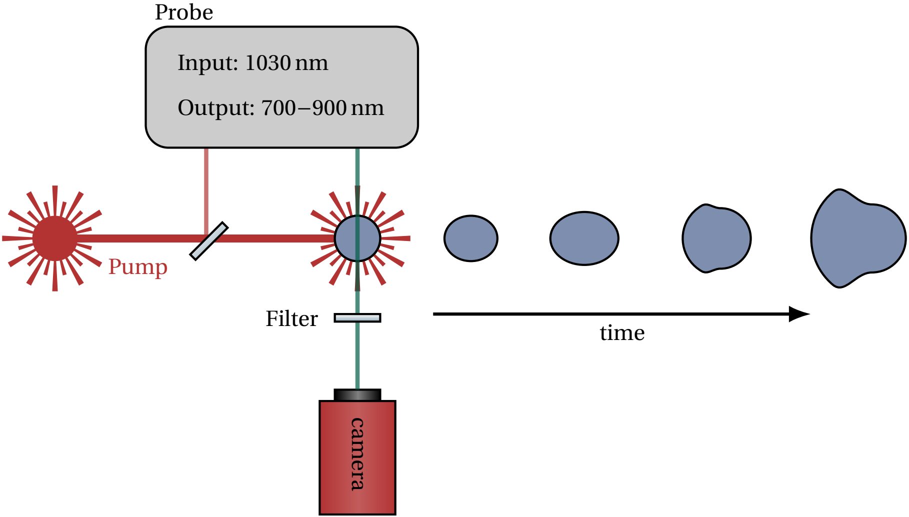
Probe
Input: 1030 nm
Output: 700–900 nm
Pump
Filter
camera
time

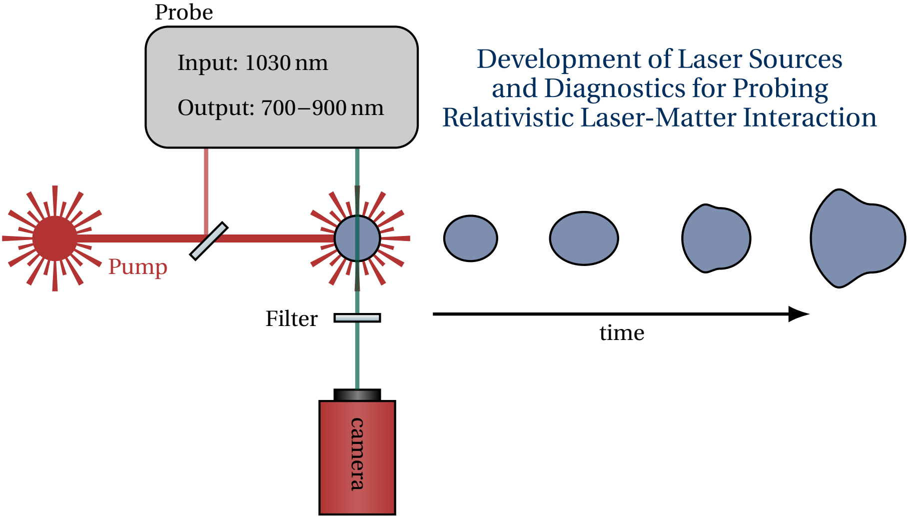

Development of Laser Sources and Diagnostics for Probing Relativistic Laser-Matter Interaction

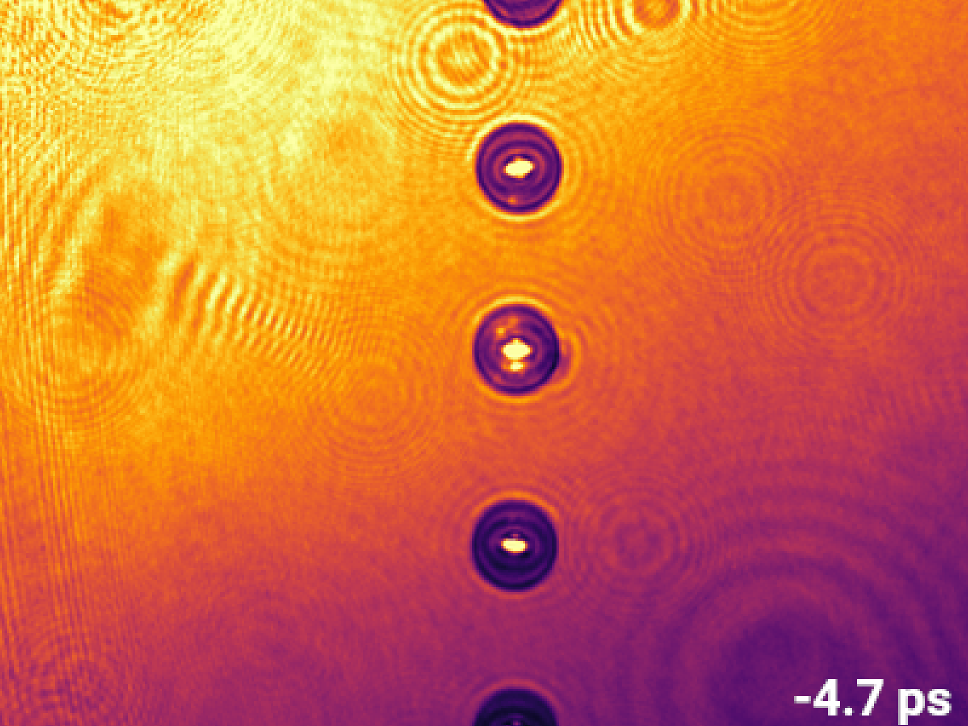
-4.7 ps

Outline

1. Fundamentals
   - Laser-induced plasmas
   - Optical parametric amplification
2. Probing realtivistic laser-plasma interactions
3. SPM-based laser pulse generation

- Plasma: "A quasineutral gas of charged and neutral particles which exhibits collective behavior" [Chen, Introduction to plasma physics and controlled fusion]

Laser-induced plasmas

iOQ JENA
Friedrich-Schiller-Universität

- Plasma: "A quasineutral gas of charged and neutral particles which exhibits collective behavior" [Chen, Introduction to plasma physics and controlled fusion]
- classical ionization: photoelectric effect $E = \hbar\omega > E_{\text{ion}}$,
  water: $E_{\text{ion}} = 10.1\,\text{eV}$ vs. POLARIS: $E_{\text{photon}} = 1.2\,\text{eV}$

- Plasma: "A quasineutral gas of charged and neutral particles which exhibits collective behavior" [Chen, Introduction to plasma physics and controlled fusion]
- classical ionization: photoelectric effect $E = \hbar\omega > E_{\text{ion}}$, water: $E_{\text{ion}} = 10.1\,\text{eV}$ vs. POLARIS: $E_{\text{photon}} = 1.2\,\text{eV}$
- For higher intensities:

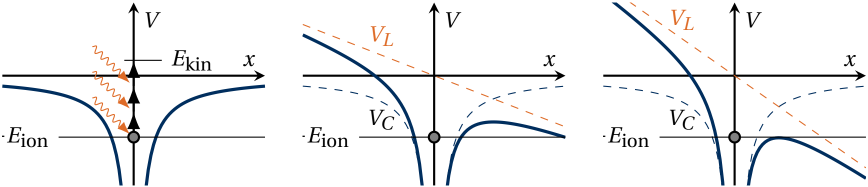

(a) Multi-Photon Ionization (b) Tunnel Ionization (c) Over the Barrier Ionization

Plasma properties

- plasma frequency: $\omega_p^2 = \dfrac{n_e e^2}{\varepsilon_0 m_e}$,

Plasma properties

- plasma frequency: $\omega_p^2 = \dfrac{n_e e^2}{\varepsilon_0 m_e}$, critical density: $n_{\text{cr}} = \dfrac{\omega^2 \varepsilon_0 m_e}{e^2}$

  $\Rightarrow$ plasma is opaque for wavelengths above $\lambda = 2\pi c/\omega_p$

Plasma properties

- plasma frequency: $\omega_p^2 = \dfrac{n_e e^2}{\varepsilon_0 m_e}$, critical density: $n_{\rm cr} = \dfrac{\omega^2 \varepsilon_0 m_e}{e^2}$

  $\Rightarrow$ plasma is opaque for wavelengths above $\lambda = 2\pi c/\omega_p$

- Plasma expansion:

plasma scale length → L; ions sound speed → c_s

$$n_e(x,t) = n_{e0} \exp\left(-\frac{x}{L}\right) \quad \text{with} \quad L = c_s \cdot t \quad \text{and} \quad c_s = \sqrt{\frac{k_B T_e Z}{m_i}}$$

n_{e0}: plasma density at $t = 0$

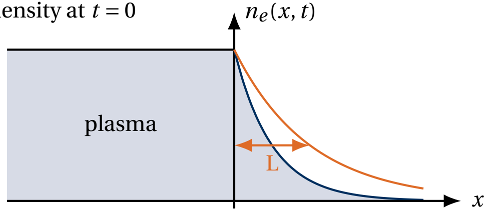

(a)

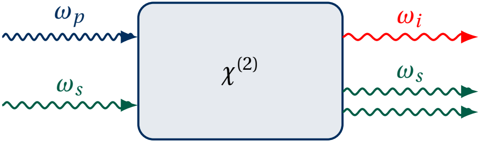

Fig.: Process of Difference frequency generation (DFG).
(a) Geometry. conversion of the pump photon ω_p to ω_s and $\omega_i = \omega_p - \omega_s$.

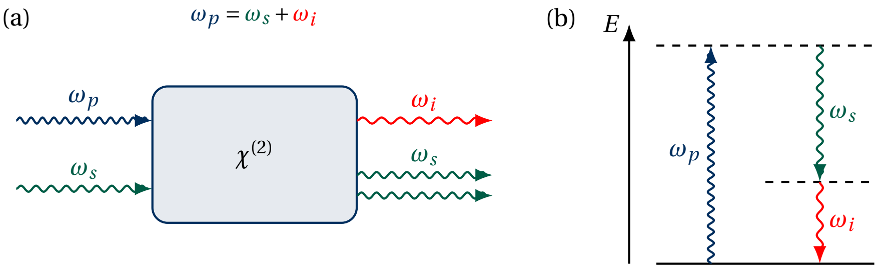

Fig.: Process of Difference frequency generation (DFG).
(a) Geometry. conversion of the pump photon ω_p to ω_s and $\omega_i = \omega_p - \omega_s$.
(b) Energy-level description.

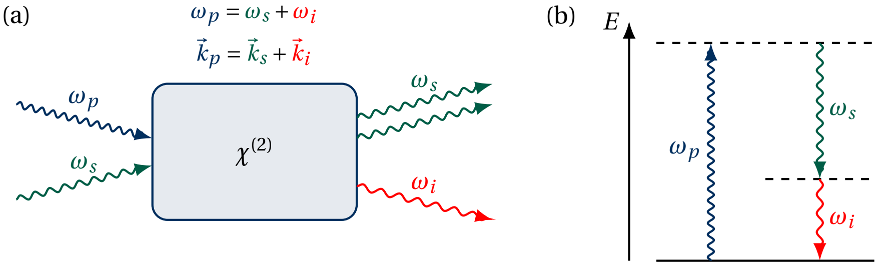

Fig.: Process of Difference frequency generation (DFG).
(a) Geometry. conversion of the pump photon ω_p to ω_s and $\omega_i = \omega_p - \omega_s$.
(b) Energy-level description.

Outline

Specifications of a probe pulse laser

- **Pulse duration** $\tau < 130\,\mathrm{fs}$
  $\Rightarrow$ high temporal resolution

Specifications of a probe pulse laser

iOQ JENA
Friedrich-Schiller-Universität

- **Pulse duration** $\tau < 130\,\text{fs}$
  $\Rightarrow$ high temporal resolution
- **Wavelength** $\lambda = 800\,\text{nm}$
  $\Rightarrow$ No overlap with fundamental (1030 nm) and SH (515 nm) of the POLARIS laser

Specifications of a probe pulse laser

- **Pulse duration** $\tau < 130\,\text{fs}$
  $\Rightarrow$ high temporal resolution
- **Wavelength** $\lambda = 800\,\text{nm}$
  $\Rightarrow$ No overlap with fundamental (1030 nm) and SH (515 nm) of the POLARIS laser
- **Spectral bandwidth** $\Delta\lambda > 100\,\text{nm}$
  $\Rightarrow$ Support femtosecond pulse durations, enable spectrally resolved probing options

Specifications of a probe pulse laser

- **Pulse duration** $\tau < 130\,\text{fs}$
  $\Rightarrow$ high temporal resolution
- **Wavelength** $\lambda = 800\,\text{nm}$
  $\Rightarrow$ No overlap with fundamental (1030 nm) and SH (515 nm) of the POLARIS laser
- **Spectral bandwidth** $\Delta\lambda > 100\,\text{nm}$
  $\Rightarrow$ Support femtosecond pulse durations, enable spectrally resolved probing options
- **Energy** $E > 10\,\mu\text{J}$
  $\Rightarrow$ proper illumination of the interaction region without target ionization

NOPA setup

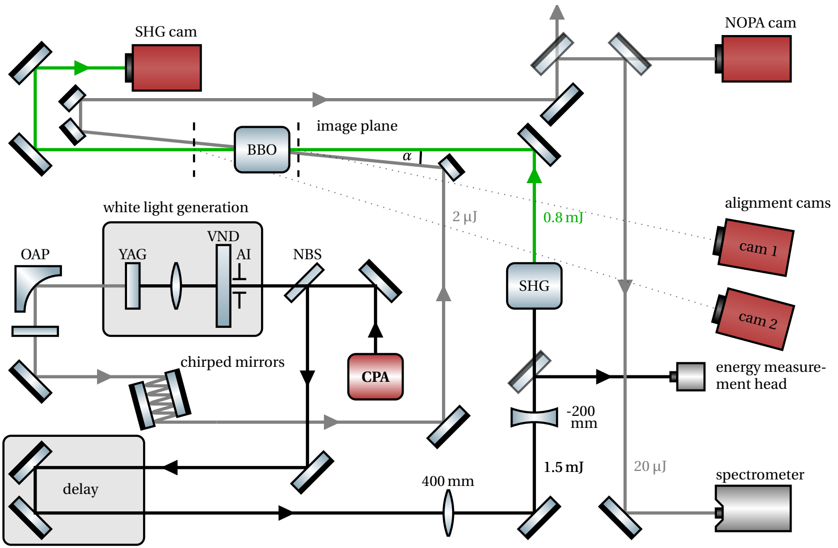

SHG cam
NOPA cam
image plane
BBO
α
white light generation
2 µJ
0.8 mJ
alignment cams
cam 1
cam 2
OAP
YAG
VND
AI
NBS
SHG
chirped mirrors
CPA
energy measure-
ment head
-200
mm
delay
400 mm
1.5 mJ
20 µJ
spectrometer

NOPA setup

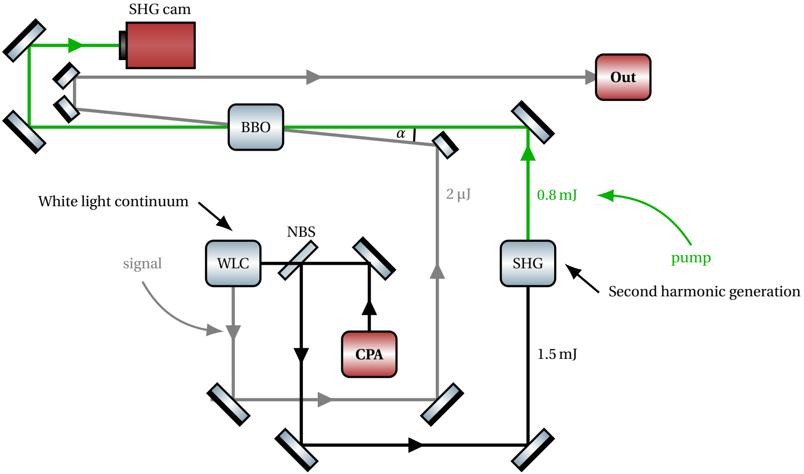
SHG cam
Out
BBO
α
2 μJ
0.8 mJ
White light continuum
NBS
WLC
signal
SHG
pump
Second harmonic generation
CPA
1.5 mJ

Spectral measurement

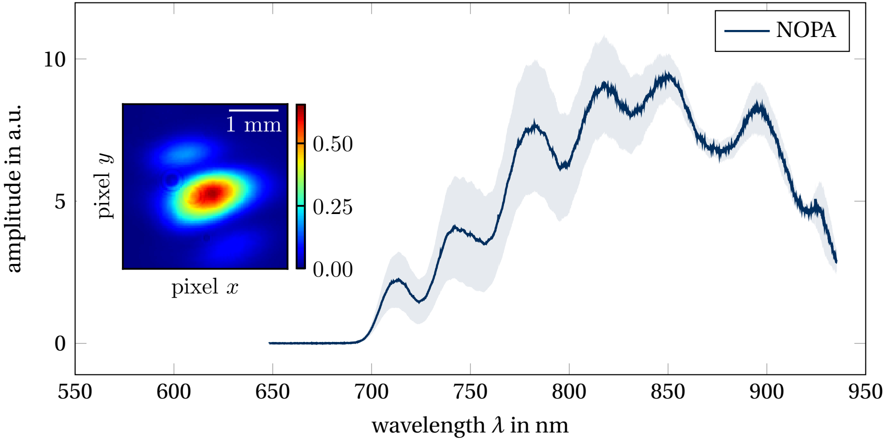

Fig.: Measured averaged spectrum (for 60 consecutive shots) of the NOPA. The standard deviation is indicated with the shaded area. Inset: Spatial profile of the NOPA.

Specifications for the probing diagnostics

- **Suppression of the plasma emission and scattered laser light**
  - ⇒ spectral filter (bandpass centered at 800 nm)

Specifications for the probing diagnostics

- **Suppression of the plasma emission and scattered laser light**
  - ⇒ spectral filter (bandpass centered at 800 nm)
  - ⇒ polarization filter

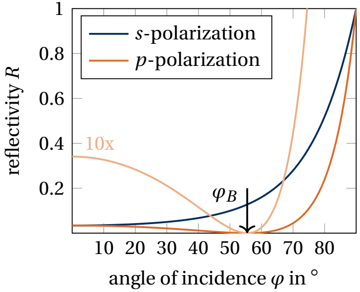

- **Suppression of the plasma emission and scattered laser light**
  - ⇒ spectral filter (bandpass centered at 800 nm)
  - ⇒ polarization filter
  - ⇒ spatial filter

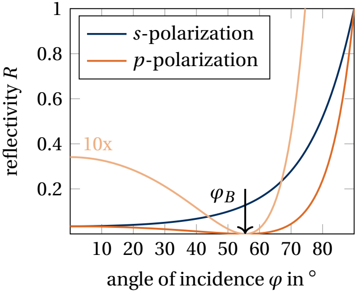

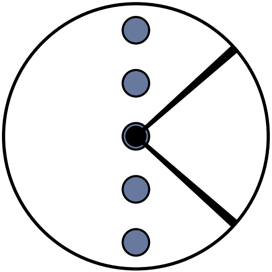

- **Suppression of the plasma emission and scattered laser light**
  - ⇒ spectral filter (bandpass centered at 800 nm)
  - ⇒ polarization filter
  - ⇒ spatial filter
- **resolution** ⇒ microscope objective

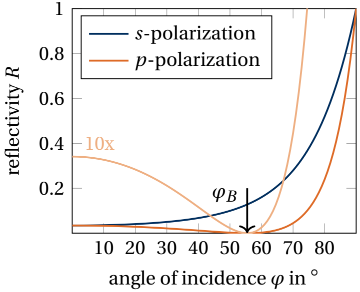

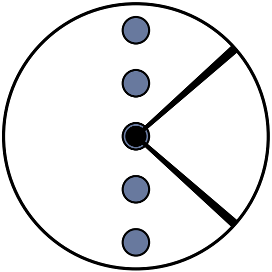

Experimental setup

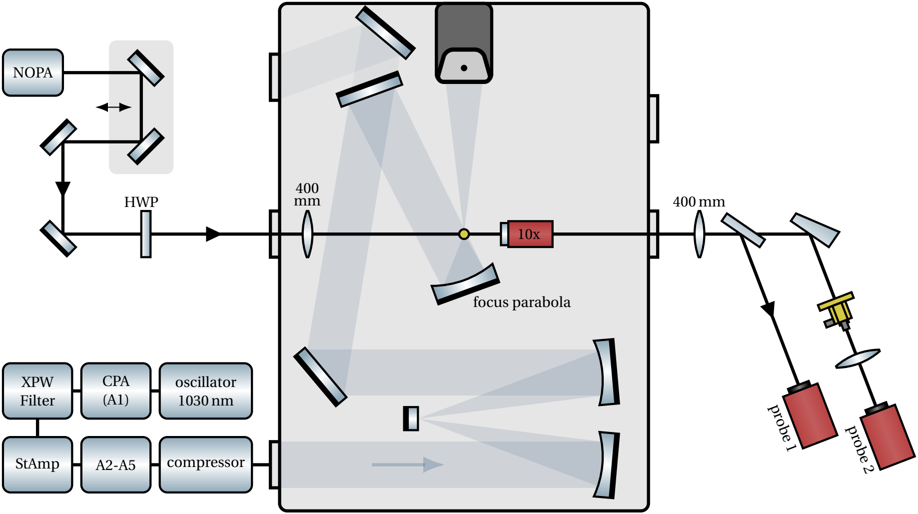

Diagnostics setup

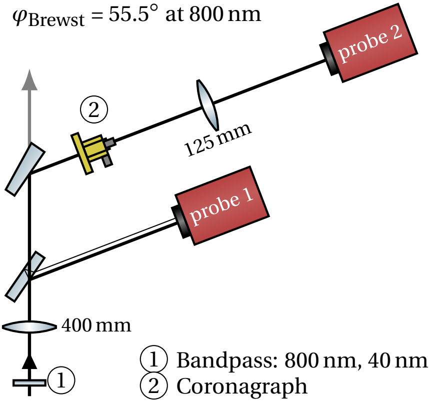

① Bandpass: 800 nm, 40 nm (FWHM)
② Coronagraph

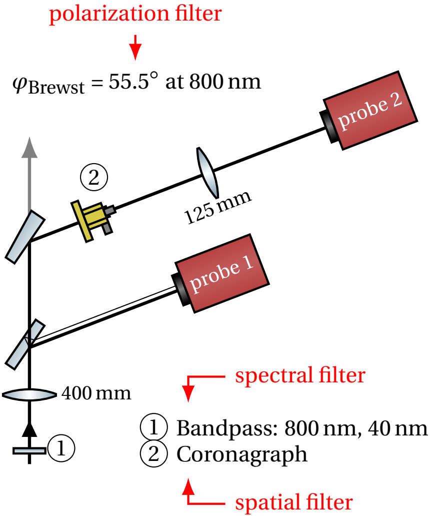

1 Bandpass: 800 nm, 40 nm (FWHM)
2 Coronagraph

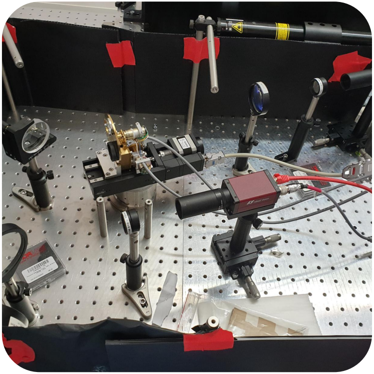

Spatial filter - Coronagraph

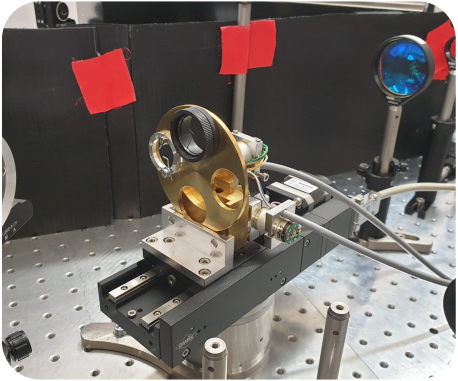

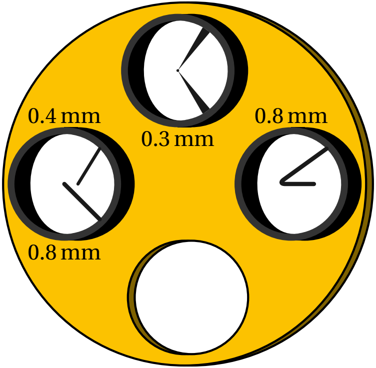

Coronagraph - Experimental results

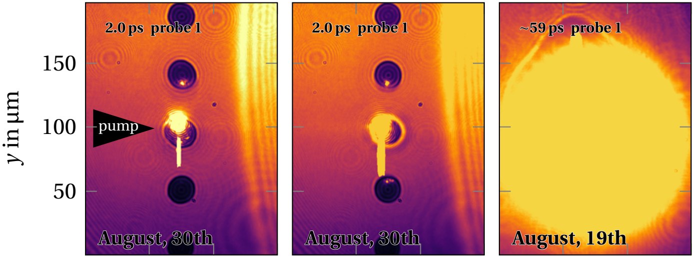

Coronagraph - Experimental results

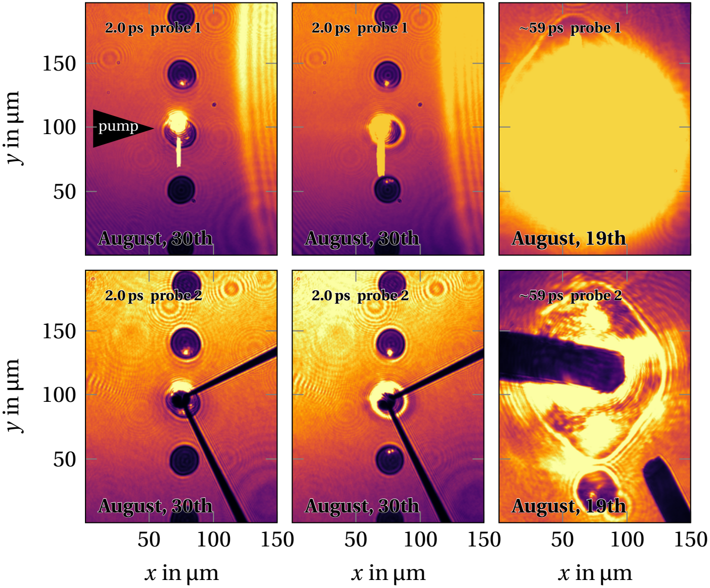

Shadowgraphy of the plasma evolution

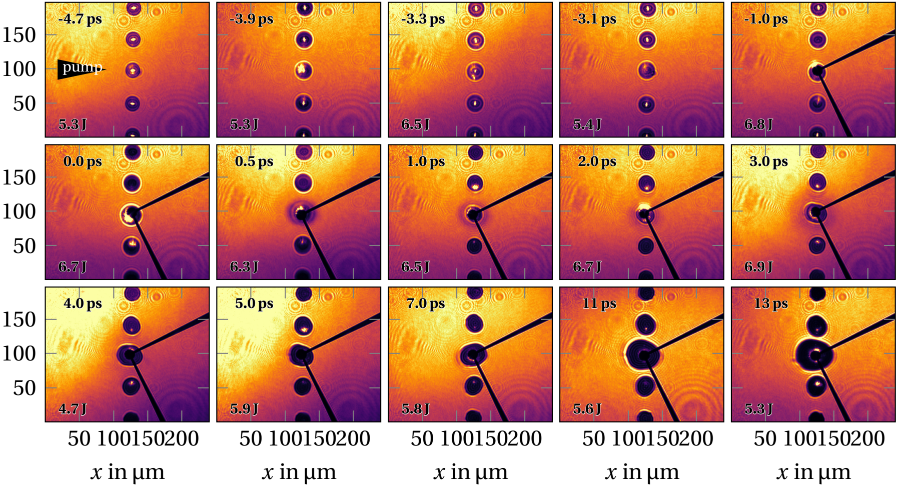

Shadowgraphy of the plasma evolution

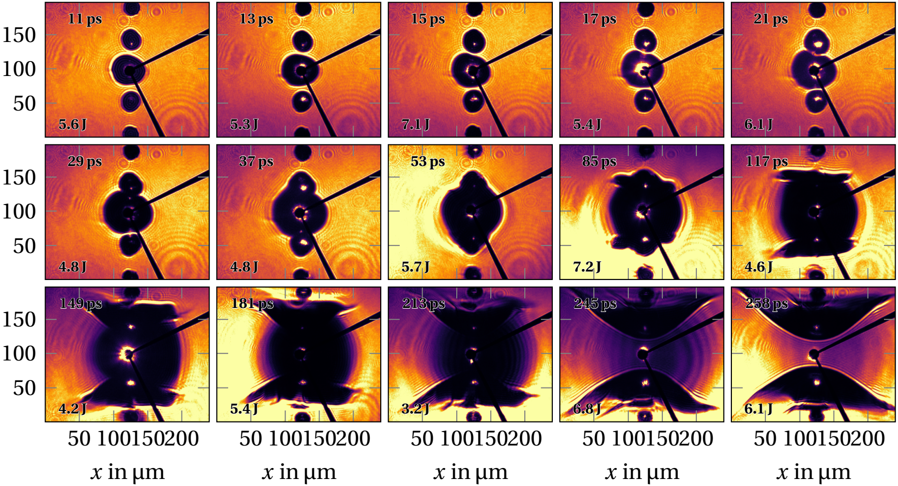

Estimation of plasma expansion velocity

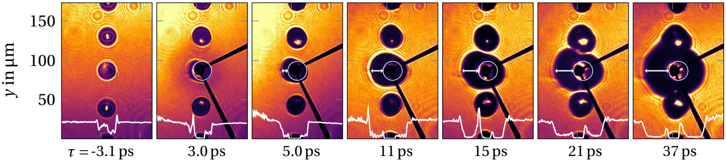

Estimation of plasma expansion velocity

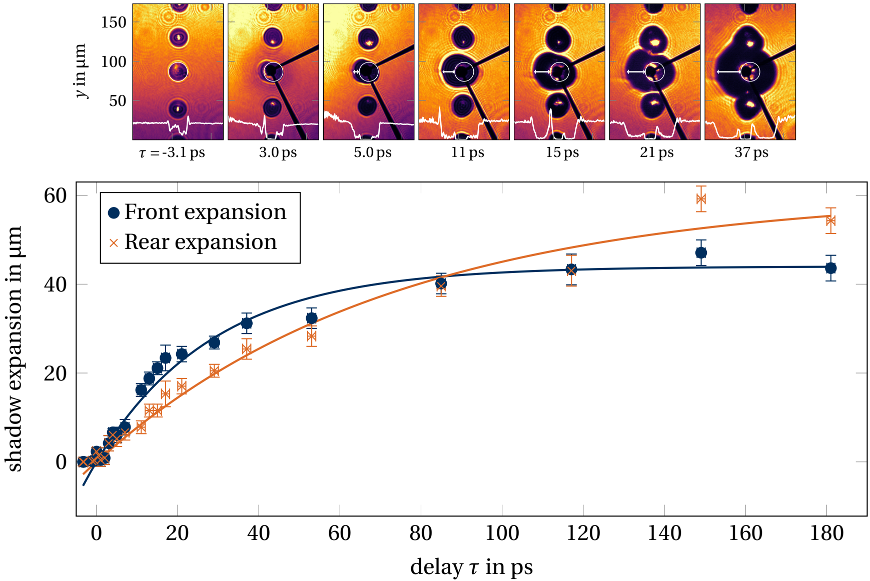

Estimation of plasma expansion velocity

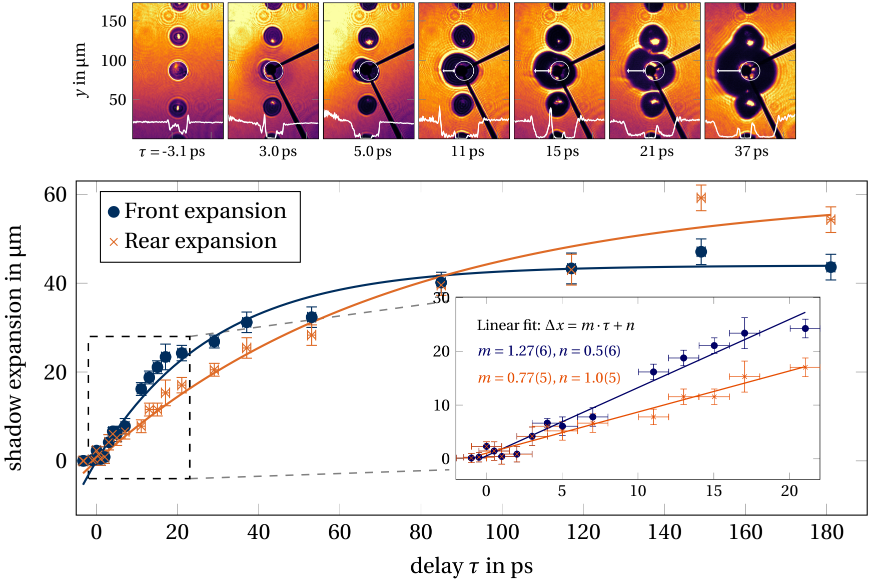

Estimation of plasma expansion velocity

$\tau = 3\text{–}20\,\text{ps} \quad v_{\text{front}} = (1.27 \pm 0.06)\,\mu\text{m/ps}, \quad v_{\text{rear}} = (0.77 \pm 0.05)\,\mu\text{m/ps}$

$\tau = 80\text{–}190\,\text{ps} \quad v_{\text{front}} = (0.09 \pm 0.03)\,\mu\text{m/ps}, \quad v_{\text{rear}} = (0.22 \pm 0.05)\,\mu\text{m/ps}.$

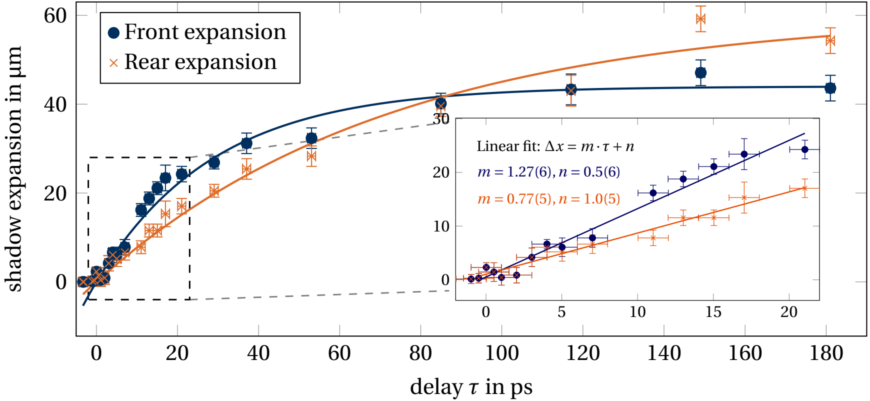

Estimation of plasma expansion velocity

$$\tau = 3\text{–}20\,\text{ps} \quad v_{\text{front}} = (1.27 \pm 0.06)\,\mu\text{m/ps}, \quad v_{\text{rear}} = (0.77 \pm 0.05)\,\mu\text{m/ps}$$

$$\tau = 80\text{–}190\,\text{ps} \quad v_{\text{front}} = (0.09 \pm 0.03)\,\mu\text{m/ps}, \quad v_{\text{rear}} = (0.22 \pm 0.05)\,\mu\text{m/ps}.$$

Table: Comparison of shadowgraphy plasma expansion experiments with targets for different peak intensities.

experiment	target	intensity	λ	v_{front}
Becker[1]	H_2O droplets	$10^{16}\,\text{W/cm}^2$	800 nm	0.38 μm/ps
This thesis	H_2O droplets	$4 \cdot 10^{19}\,\text{W/cm}^2$	1030 nm	1.3 μm/ps
Bernert et al.[2]	hydrogen jet	$5 \cdot 10^{21}\,\text{W/cm}^2$	800 nm	23 μm/ps

[1] "Characterization of laser-driven proton acceleration with contrast-enhanced laser pulses"
[2] "Off-harmonic optical probing of high intensity laser plasma expansion dynamics in solid density hydrogen jets"

Outline

Optical Kerr effect (intensity dependent refractive index)

$$n(t) = n_0 + n_2 I(t), \quad \text{where} \quad n_2 = \frac{3\chi^{(3)}}{4\varepsilon_0 n_0^2 c}.$$

Optical Kerr effect (intensity dependent refractive index)

$$n(t) = n_0 + n_2 I(t), \quad \text{where} \quad n_2 = \frac{3\chi^{(3)}}{4\varepsilon_0 n_0^2 c}.$$

Change in the phase: $\Phi_{\mathrm{NL}}(t) = n_2 I(t) k_0 L$.

Self phase modulation (SPM)

Optical Kerr effect (intensity dependent refractive index)

$$n(t) = n_0 + n_2 I(t), \quad \text{where} \quad n_2 = \frac{3\chi^{(3)}}{4\varepsilon_0 n_0^2 c}.$$

Change in the phase: $\Phi_{\mathrm{NL}}(t) = n_2 I(t) k_0 L$.

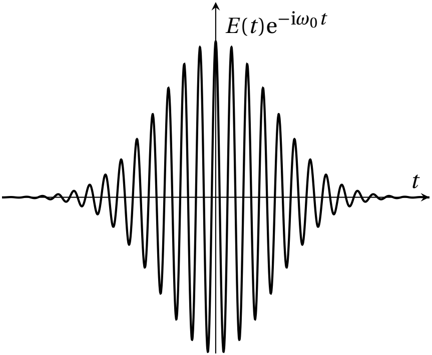

Optical Kerr effect (intensity dependent refractive index)

$$n(t) = n_0 + n_2 I(t), \quad \text{where} \quad n_2 = \frac{3\chi^{(3)}}{4\varepsilon_0 n_0^2 c}.$$

Change in the phase: $\Phi_{\mathrm{NL}}(t) = n_2 I(t) k_0 L$.

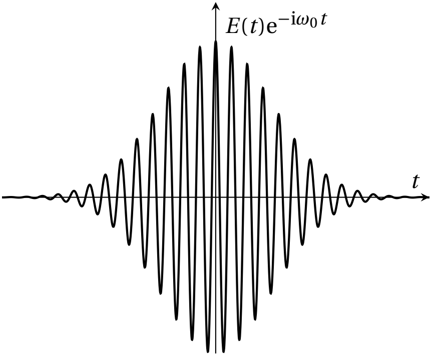

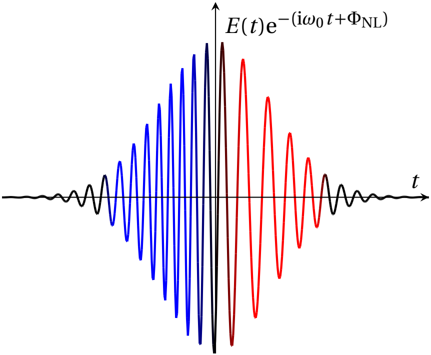

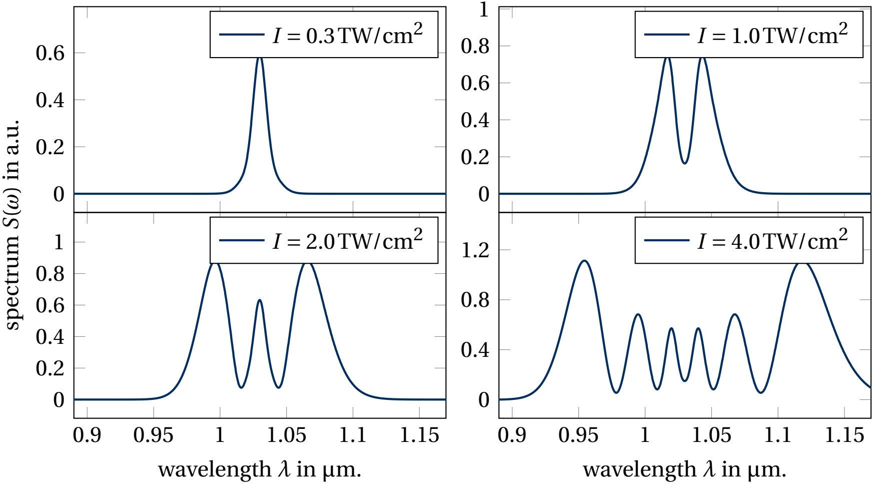

Fig.: Simulated spectra of a laser pulse with $\tau = 130\,\mathrm{fs}$ (FWHM) propagating through a 1 mm thick foil of CR-39 at different intensities.

Specifications of a probe pulse laser

- **Pulse duration** $\tau < 130\,\mathrm{fs}$
  ⇒ high temporal resolution
- **Wavelength** $\lambda = 800 - 1000\,\mathrm{nm}$
  ⇒ No overlap with fundamental (1030 nm) and SH (515 nm) of the POLARIS laser
- **Spectral bandwidth** $\Delta\lambda > 100\,\mathrm{nm}$
  ⇒ Support femtosecond pulse durations
- **Energy** $E > 10\,\mu\mathrm{J}$
  ⇒ proper illumination, no target ionization

Single-pass SPM

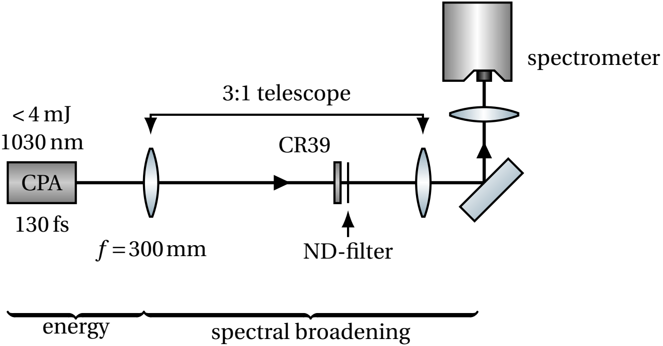

Single-pass SPM

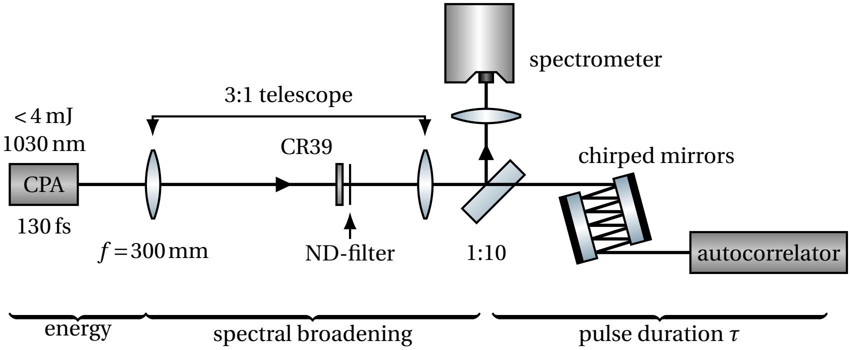

SPM - spectral measurement

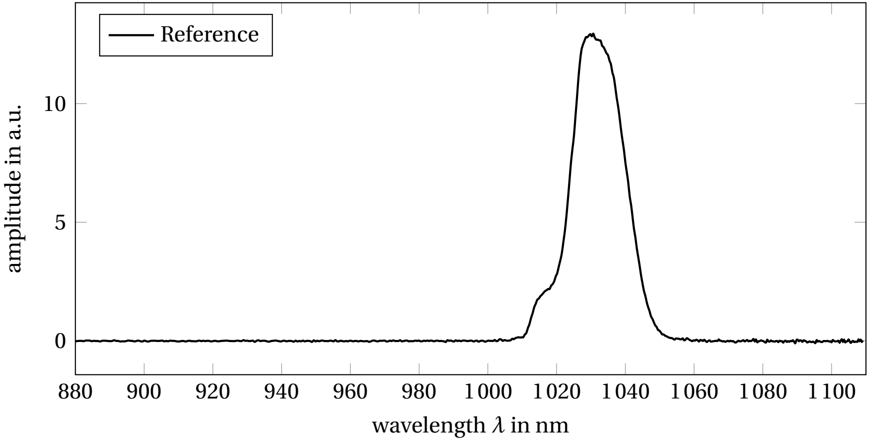

Fig.: Measurement of SPM-induced spectra in CR-39 for a pulse energy of 0.5 mJ at different intensities by varying the sample distance to the focus position. A reference spectrum in air was taken at a lower pulse energy of 0.1 mJ.

SPM - spectral measurement

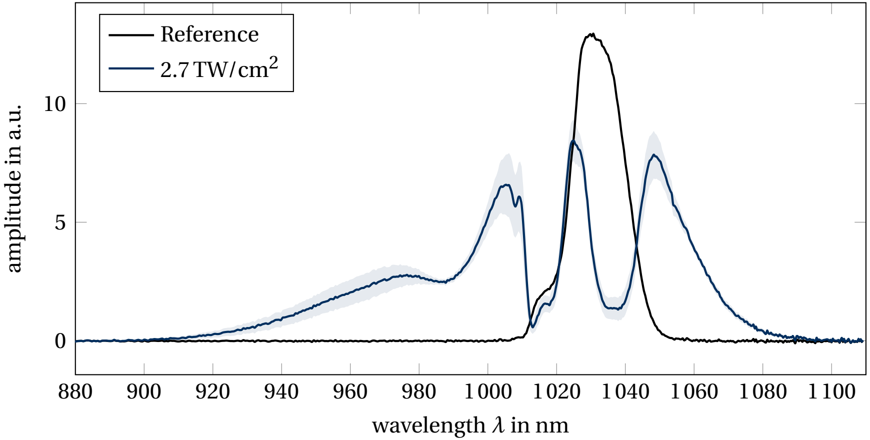

Fig.: Measurement of SPM-induced spectra in CR-39 for a pulse energy of 0.5 mJ at different intensities by varying the sample distance to the focus position. A reference spectrum in air was taken at a lower pulse energy of 0.1 mJ.

SPM - spectral measurement

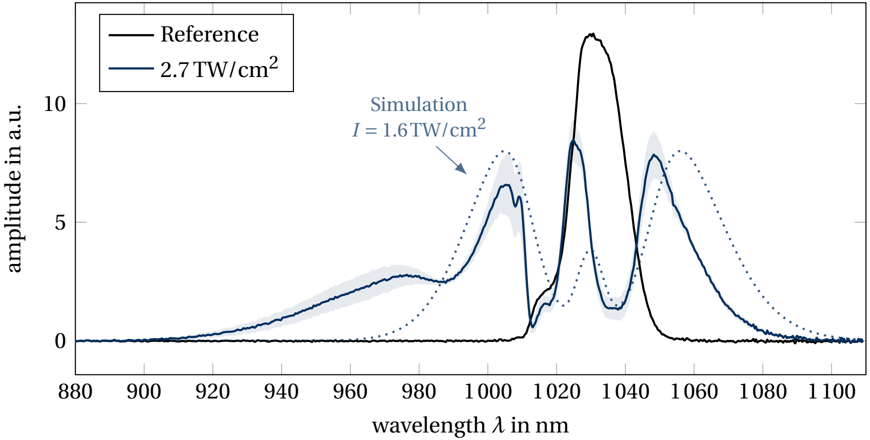

Fig.: Measurement of SPM-induced spectra in CR-39 for a pulse energy of 0.5 mJ at different intensities by varying the sample distance to the focus position. A reference spectrum in air was taken at a lower pulse energy of 0.1 mJ.

SPM - spectral measurement

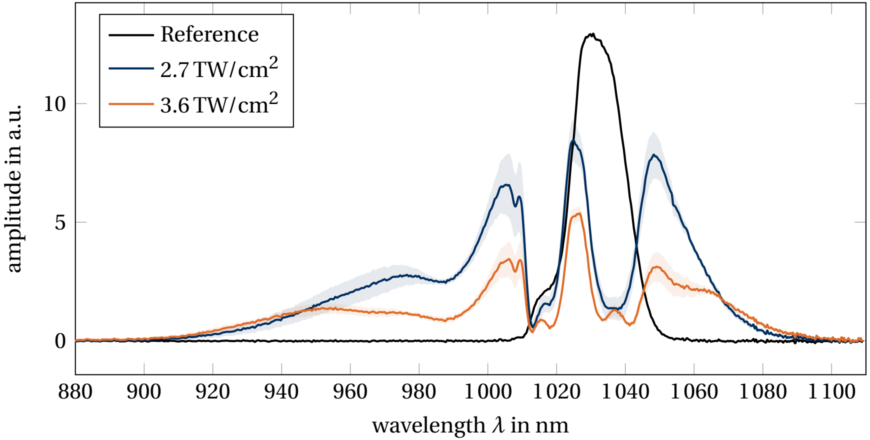

Fig.: Measurement of SPM-induced spectra in CR-39 for a pulse energy of 0.5 mJ at different intensities by varying the sample distance to the focus position. A reference spectrum in air was taken at a lower pulse energy of 0.1 mJ.

SPM - spectral measurement

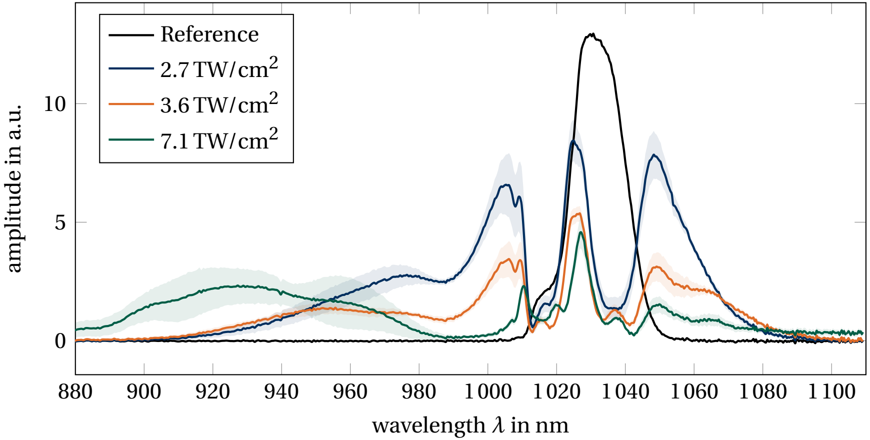

Fig.: Measurement of SPM-induced spectra in CR-39 for a pulse energy of 0.5 mJ at different intensities by varying the sample distance to the focus position. A reference spectrum in air was taken at a lower pulse energy of 0.1 mJ.

SPM - energy measurement

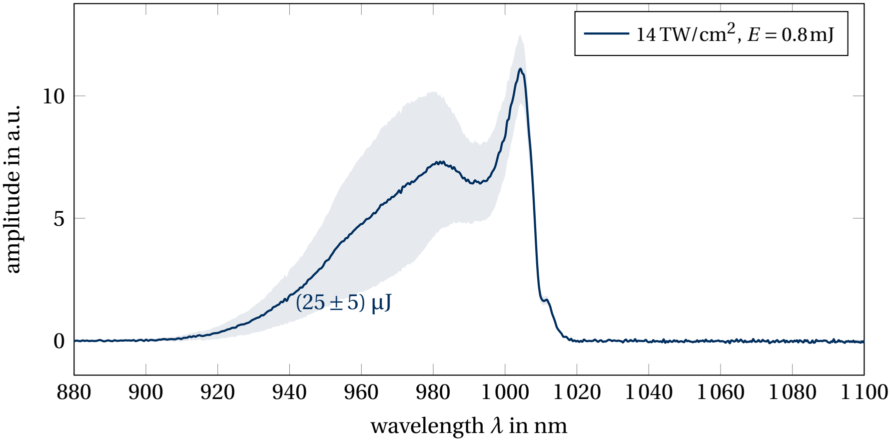

Fig.: Measurement of SPM in CR-39 performed at low pressure (5 mbar) with a short-pass filter cutting at 1010 nm.

SPM - energy measurement

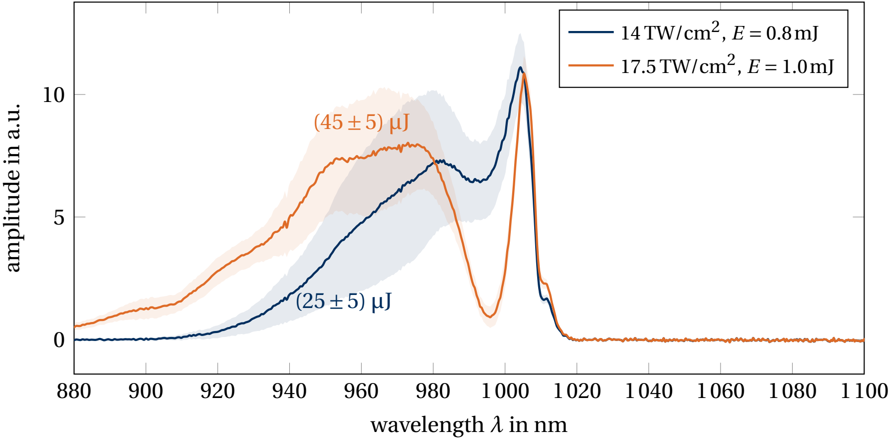

Fig.: Measurement of SPM in CR-39 performed at low pressure (5 mbar) with a short-pass filter cutting at 1010 nm.

SPM - energy measurement

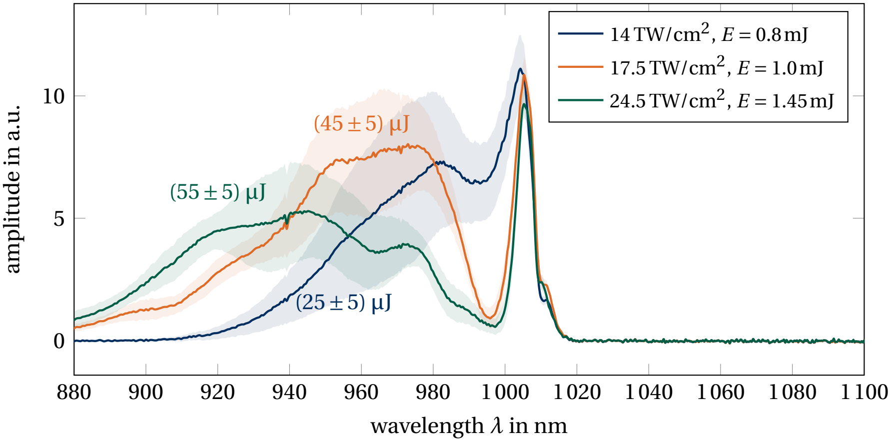

Fig.: Measurement of SPM in CR-39 performed at low pressure (5 mbar) with a short-pass filter cutting at 1010 nm.

Multi-pass cell

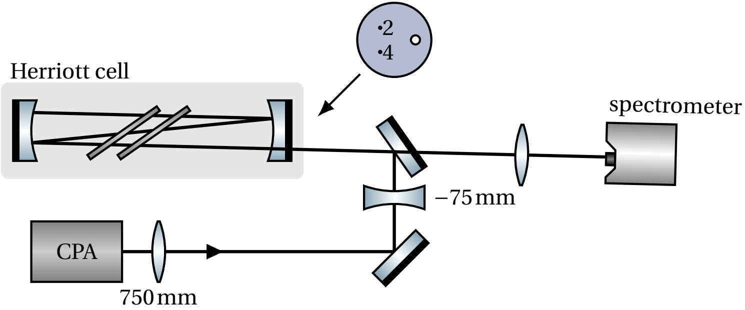

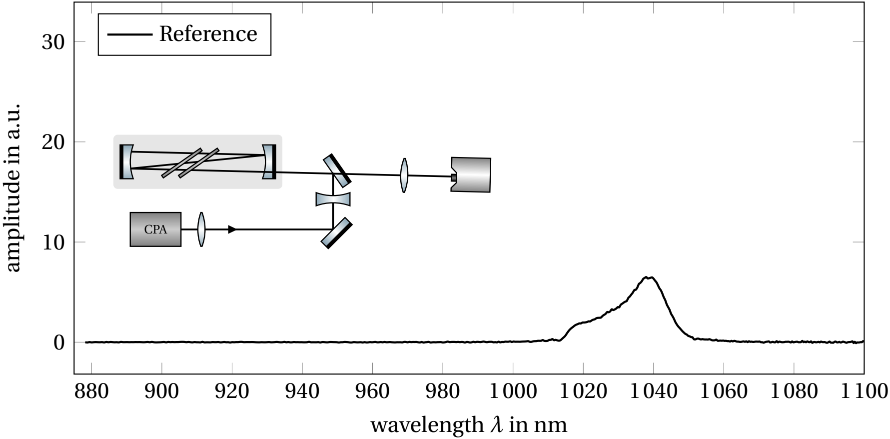

Fig.: Measured Spectra in two samples of 1.1 mm CR-39 placed in the Brewster angle into a MPC of length $L = 10\,\text{cm}$.

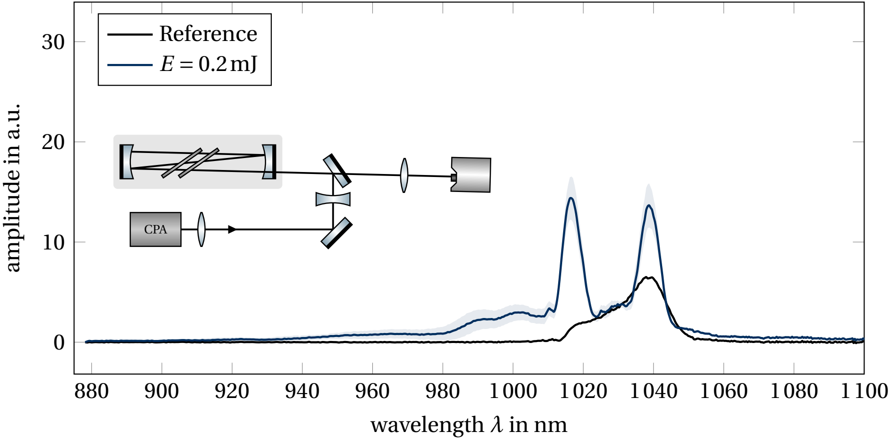

Fig.: Measured Spectra in two samples of 1.1 mm CR-39 placed in the Brewster angle into a MPC of length $L = 10\,\text{cm}$.

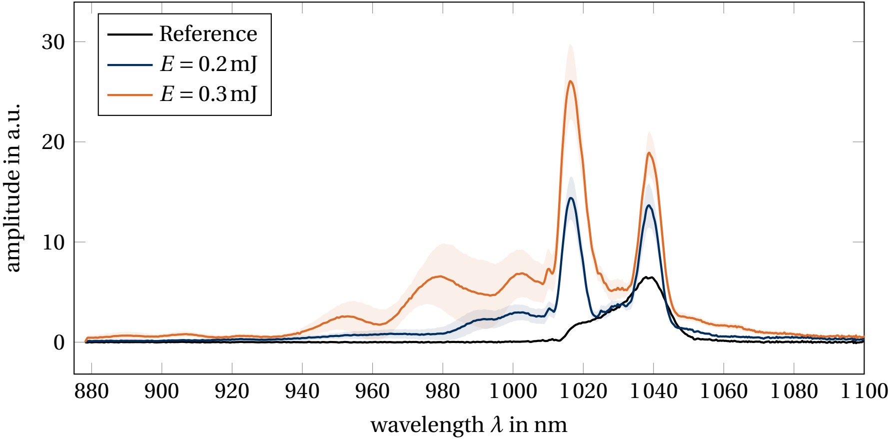

Fig.: Measured Spectra in two samples of 1.1 mm CR-39 placed in the Brewster angle into a MPC of length $L = 10\,\text{cm}$.

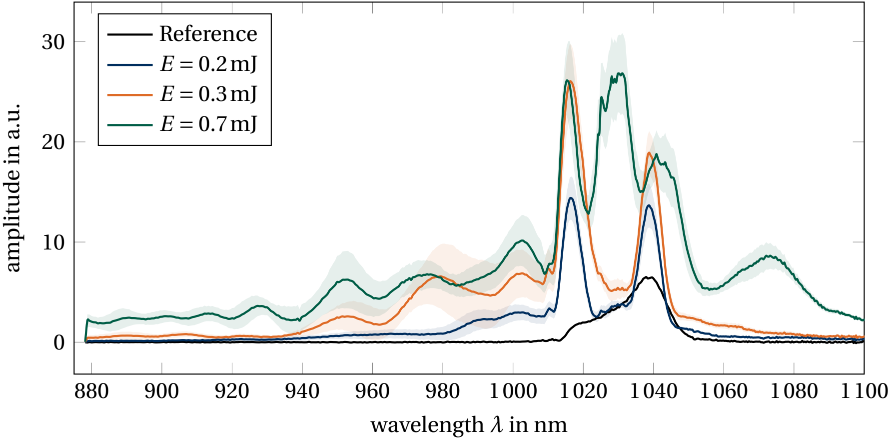

Fig.: Measured Spectra in two samples of 1.1 mm CR-39 placed in the Brewster angle into a MPC of length $L = 10\,\mathrm{cm}$.

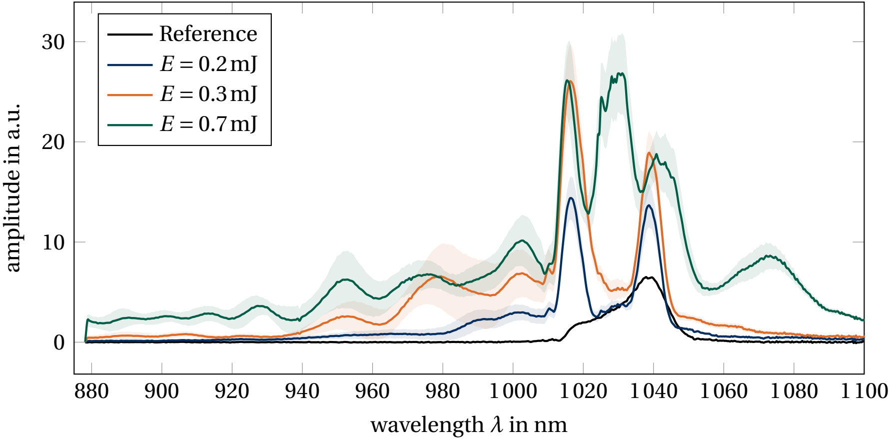

Fig.: Measured Spectra in two samples of 1.1 mm CR-39 placed in the Brewster angle into a MPC of length $L = 10\,\mathrm{cm}$.

Pulse steepening - temporal domain

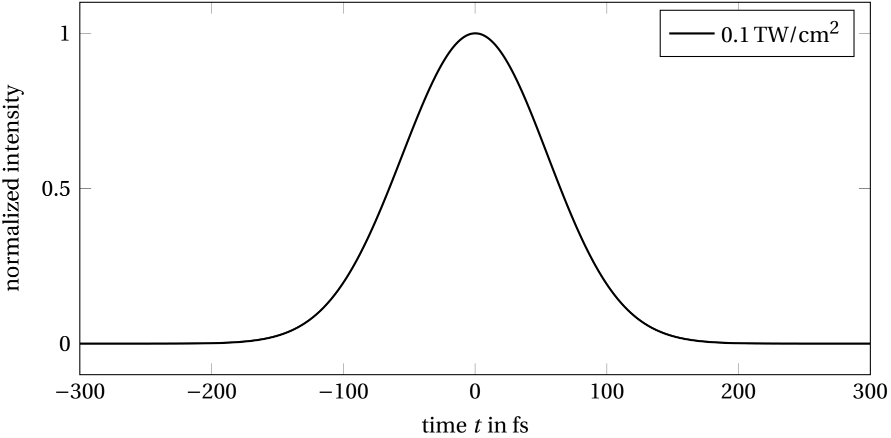

Fig.: Simulated temporal profiles of the pulse intensities for a 1.1 mm thick sheet of CR-39 with an initial pulse length of 130 fs (FWHM) for different intensities.

Pulse steepening - temporal domain

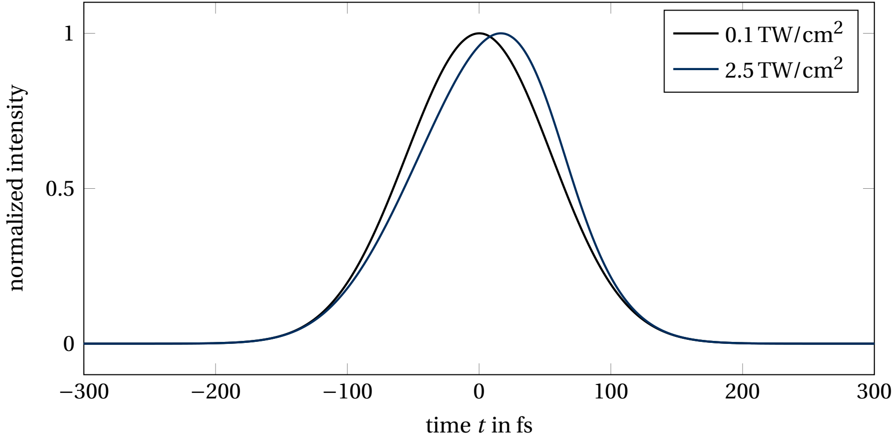

Fig.: Simulated temporal profiles of the pulse intensities for a 1.1 mm thick sheet of CR-39 with an initial pulse length of 130 fs (FWHM) for different intensities.

Pulse steepening - temporal domain

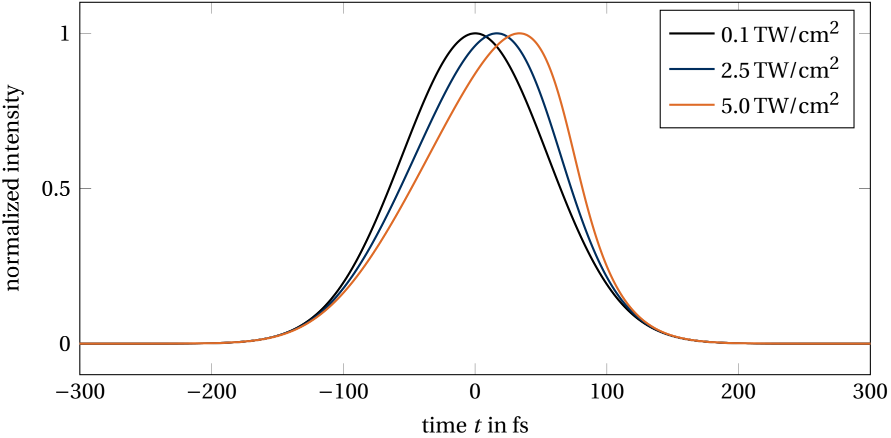

Fig.: Simulated temporal profiles of the pulse intensities for a 1.1 mm thick sheet of CR-39 with an initial pulse length of 130 fs (FWHM) for different intensities.

Pulse steepening - temporal domain

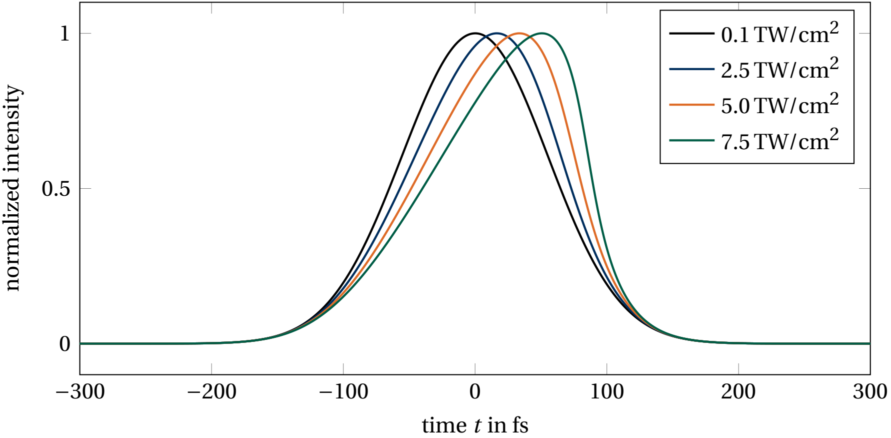

Fig.: Simulated temporal profiles of the pulse intensities for a 1.1 mm thick sheet of CR-39 with an initial pulse length of 130 fs (FWHM) for different intensities.

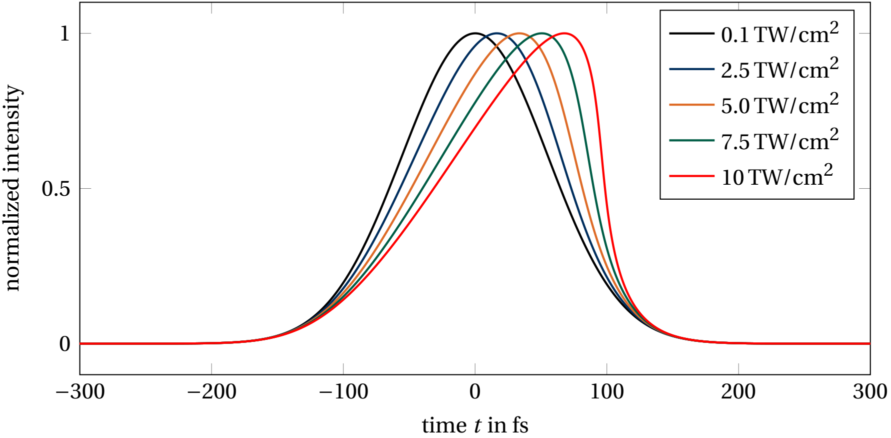

Fig.: Simulated temporal profiles of the pulse intensities for a 1.1 mm thick sheet of CR-39 with an initial pulse length of 130 fs (FWHM) for different intensities.

Pulse steepening - spectral domain

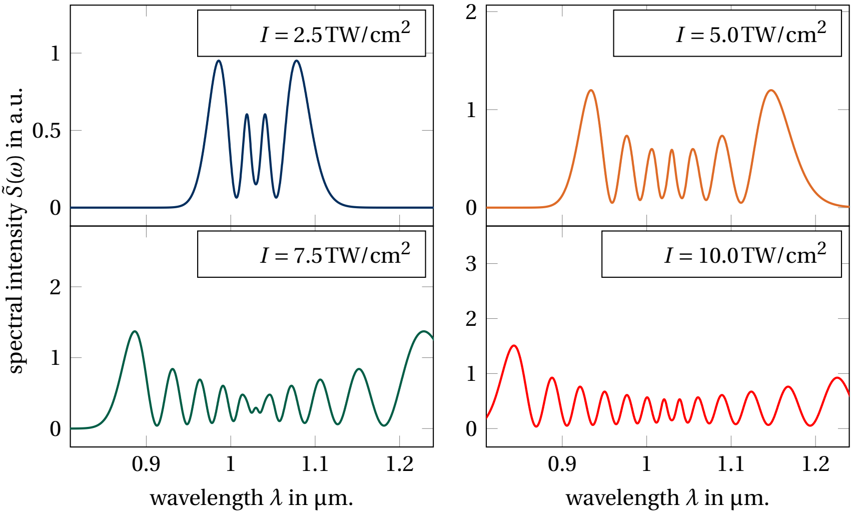

Fig.: Calculated spectra of an ultrashort pulse propagating through CR-39.

Pulse steepening - spectral domain

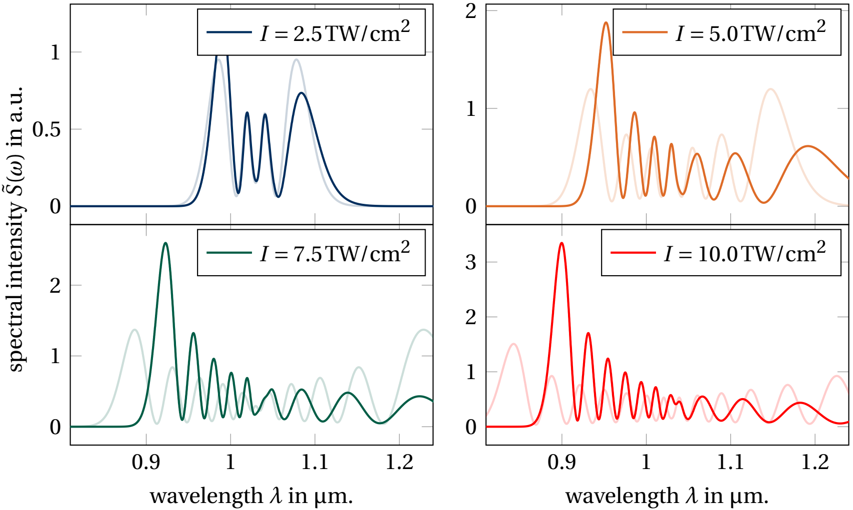

Fig.: Calculated spectra of an ultrashort pulse propagating through CR-39.

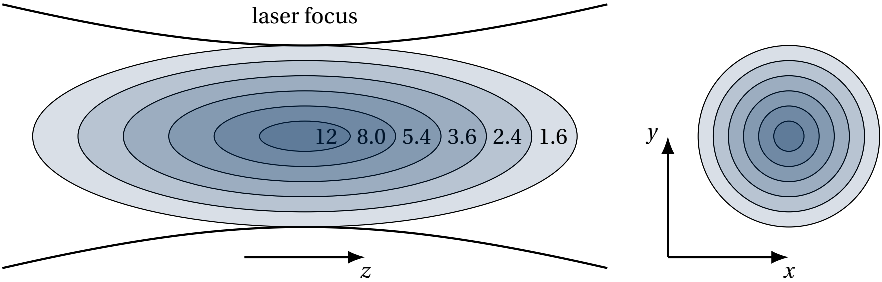

$$S(\lambda) = \frac{1}{r_N} \sum_{i=1}^{N} r_i \cdot S_i(\lambda)$$

Fig.: In a simplified model, the intensity distribution can be approximated as rings of constant thickness. The corresponding intensity drops according to the Gaussian distribution exponentially.

Focal volume averaging - simulation

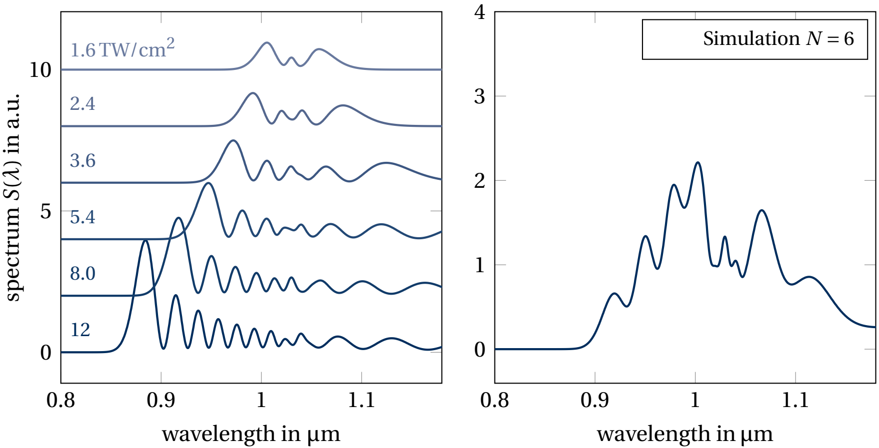

Fig.: Left: Calculated spectra including the effect of pulse steepening in CR-39.
Right: Focal volume averaging for a transverse Gaussian intensity distribution.

Focal volume averaging - simulation

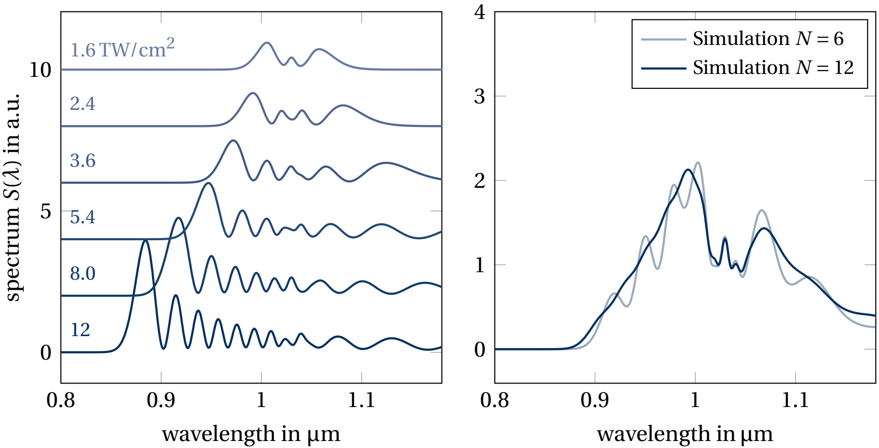

Fig.: Left: Calculated spectra including the effect of pulse steepening in CR-39.
Right: Focal volume averaging for a transverse Gaussian intensity distribution.

Focal volume averaging - simulation

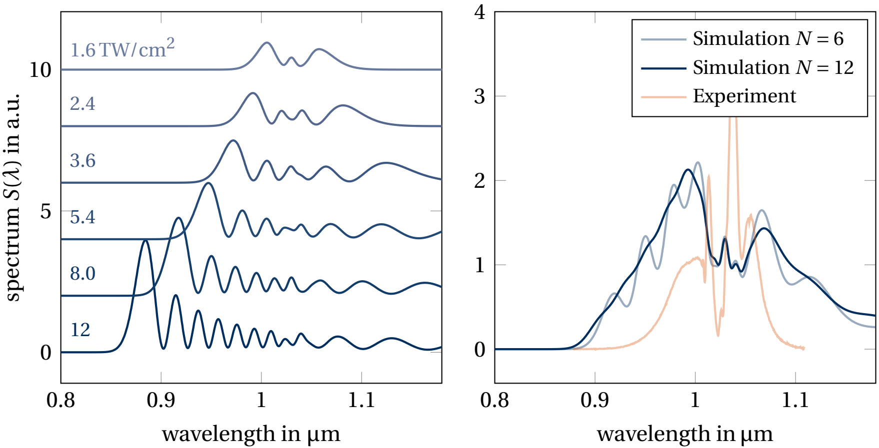

Fig.: Left: Calculated spectra including the effect of pulse steepening in CR-39.
Right: Focal volume averaging for a transverse Gaussian intensity distribution.

Probing of laser-microdroplet interaction

- characterization of the NOPA setup
- development: imaging diagnostics + coronagraph
- plasma evolution + plasma expansion velocity

Development of a new probe pulse laser source

- Single-pass SPM $\Rightarrow$ 50 µJ pulses
- Multi-pass SPM $\Rightarrow$ lower intensities
- Simulation: Pulse steepening + focal averaging

Acknowledgements

A special thanks to my supervisors:

- Prof. Dr. Malte Kaluza
- Dr. Yasmina Azamoum

I would also like to thank:

- Till Weickhardt
- Mathis Nolte
- Marco Hellwing
- Dr. Georg Becker
- Dr. Marco Hornung
- Dr. Matthew Schwab

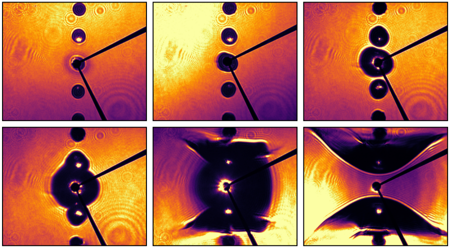

Thank you for your attention.

Phase matching for the NOPA

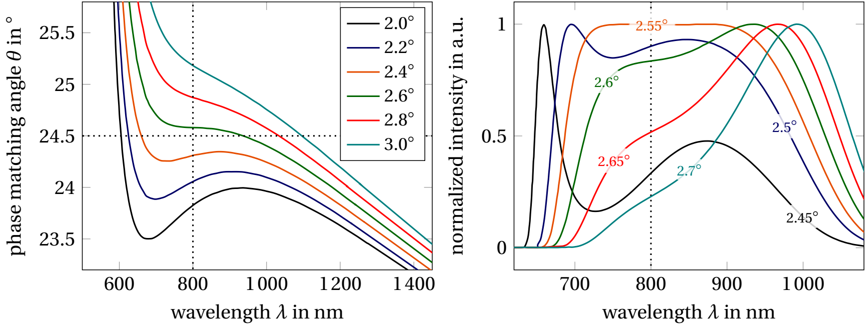

Fig.: Left: Type-1 phase-matching angle θ as a function of the signal wavelength λ_s for different pump-signal angles α with a pump wavelength at 515 nm.
Right: Calculated gain spectra for a phase matching angle of $\theta = 24.5°$ as a function of signal wavelength λ_s for different pump-signal angles α.

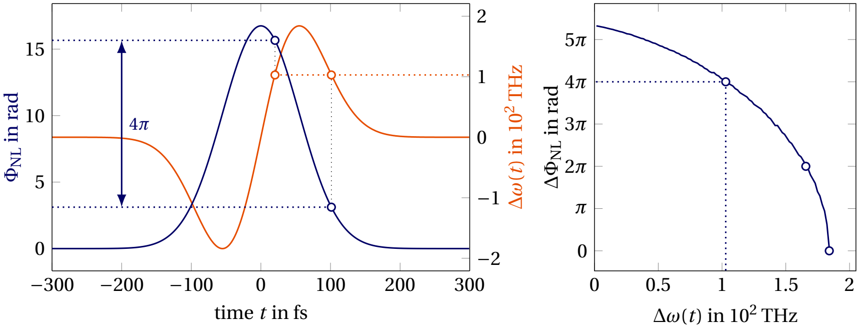

Fig.: Left: Nonlinear phase (blue) for a pulse with $\tau = 130\,\text{fs}$ (FWHM) of peak intensity $I_0 = 4\,\text{TW/cm}^2$ for 1 mm of CR-39. The instantaneous frequency change $\Delta\omega = -\frac{\partial\Phi_{NL}}{\partial t}$ is shown in orange. Right: Calculated phase difference as a function of instantaneous frequency change.

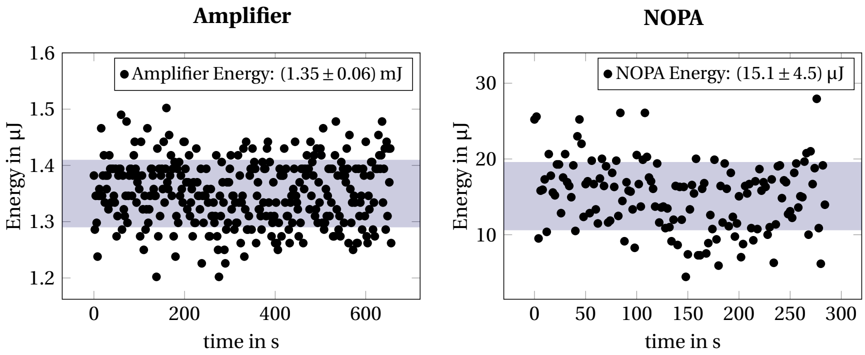

Fig.: Stability measurement of the amplifier and NOPA energy over a duration of several minutes.

Spectral control of the NOPA

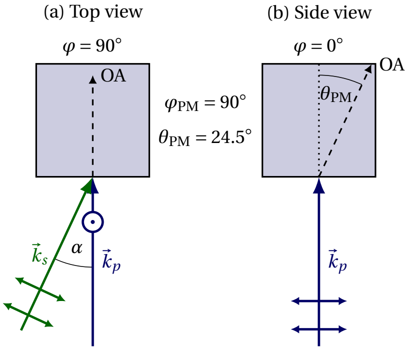

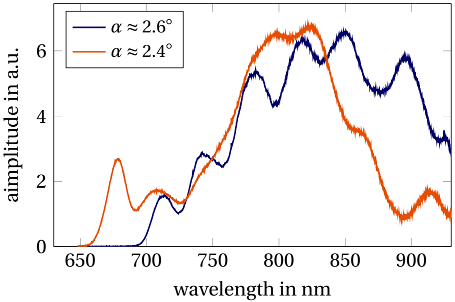

Fig.: Left: Geometry of the WLC (signal) and SH (pump) beams in the NOPA crystal (Type I o-o-e phase matching process). Right: NOPA spectra for different non-collinear angles α. The orange curve indicates that the spectral bandwidth can be reduced by an adjustment of the non-collinear angle and subsequent optimization of the temporal delay τ.

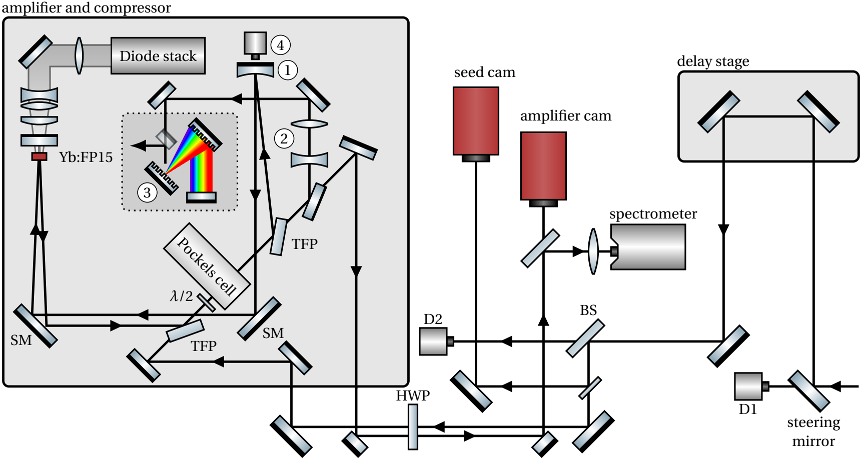
amplifier and compressor
Diode stack
4
1
2
3
Yb:FP15
TFP
Pockels cell
λ/2
SM
TFP
SM
seed cam
amplifier cam
spectrometer
delay stage
D2
BS
HWP
D1
steering mirror

CPA system - spectral measurement

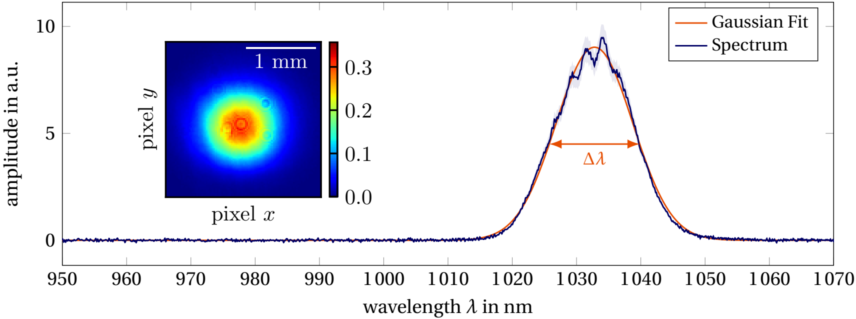

Fig.: Measured spectrum of the Amplifier. The graph shows the averaged spectrum for 80 consecutive shots. The standard deviation is indicated with the shaded area. The central wavelength $\lambda_0 = 1032.8\,\text{nm}$, and width $\Delta\lambda = 14.1\,\text{nm}$ (FWHM) were determined using a Gaussian fit (orange). Inset: spatial profile of the amplified pulse. The beam radius was determined to be $w = (0.77 \pm 0.02)\,\text{mm}\ (1/\text{e}^2)$.

CPA system - autocorrelation measurement

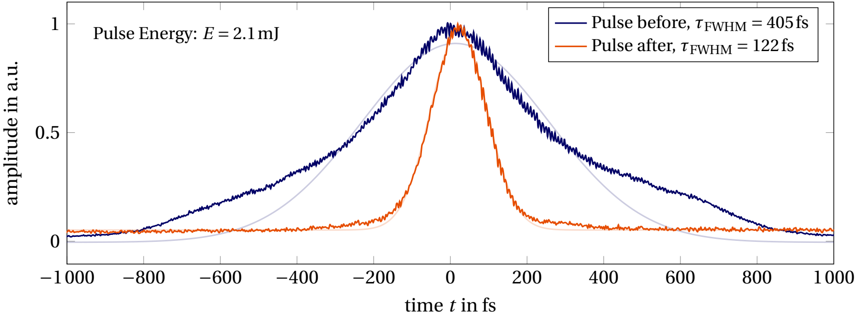

Fig.: Measured pulse length at the compressor output before (blue) and after (orange) the realignment of the stretcher. The autocorrelation function was measured by TOPAG ASF-15 single shot autocorrelator. The desaturated curves show a Gaussian fit to the measured data used to determine the pulse length.

Probing Imaging system

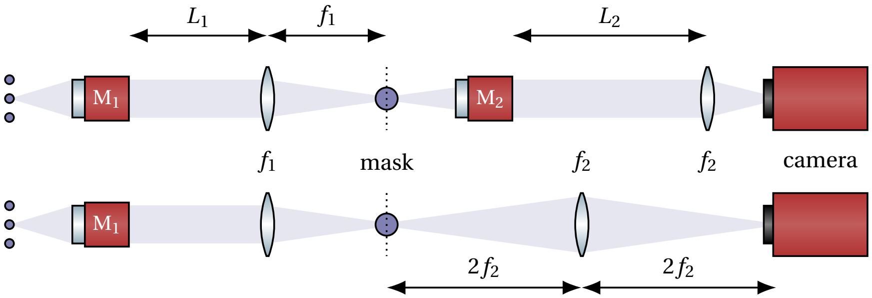

Fig.: Two different designs for a coronagraph imaging setup. Top: The droplets are magnified and imaged to the position of the coronagraph mask using an aberration corrected microscope objective M_1 and a tube lens (f_1) placed in a distance L_1 to the objective. The droplet with the blocked center is then re-imaged into a camera with another combination of objective and lens f_2 placed in a distance L_2. Bottom: The second imaging of the droplet into the camera is done by a single lens with a magnification of 1.

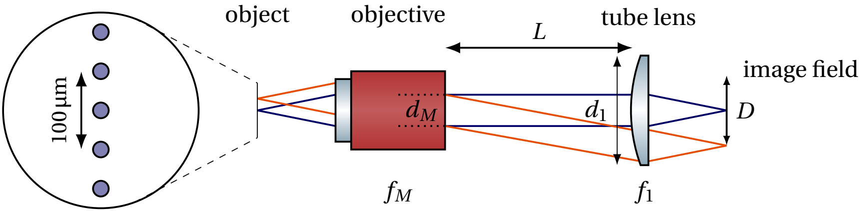

Fig.: Supplemental drawing for the placement of objective and tube lens. The maximum distance L for a desired image field D can be derived geometrically from the tube lens diameter d_1 and objective aperture d_M. The required field of view with a size of 300 µm is shown on the left.

Self focusing considerations

Self-focusing distance z_{sf}:

$$z_{sf} = \frac{2n_0 w_0^2}{\lambda_0} \frac{1}{\sqrt{P/P_{cr} - 1}} \quad \text{with} \quad P_{crit} \approx \frac{\lambda_0^2}{8n_0 n_2} = 1.42\,\mathrm{MW} \quad \text{at } \lambda_0 = 1030\,\mathrm{nm},$$

Table: Self focusing distance z_{sf} and pulse width w_0 for different pulse energies ($\tau = 130\,\mathrm{fs}$) calculated at a constant peak intensity $I = 10\,\mathrm{TW/cm^2}$.

Energy [mJ]	0.1	0.5	1	2	5
pulse radius w_0 [µm]	48	107	152	214	339
self-focusing distance z_{sf} [mm]	0.30	0.66	0.94	1.32	2.09

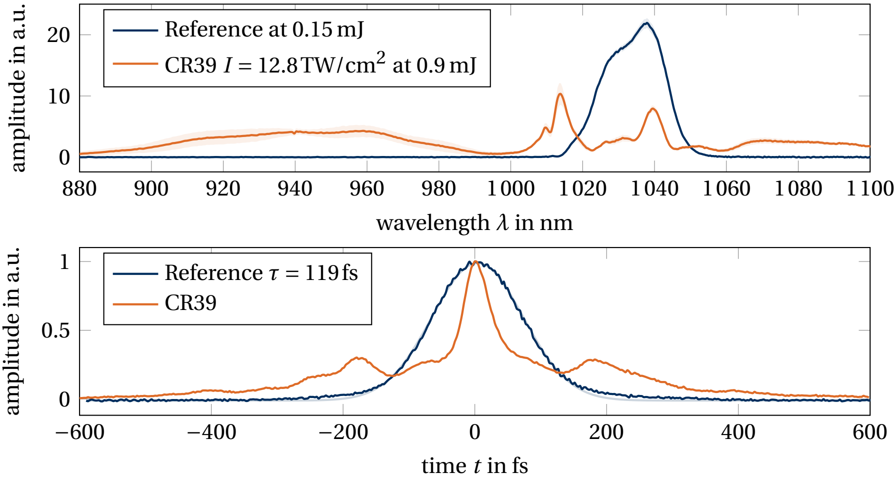

Fig.: Top: Spectra of a reference pulse (blue) and for for pulses experiencing SPM in CR-39 (orange) recorded simultaneously with an autocorrelation measurement. Bottom: Measured Autocorrelation functions.

iOQ JENA
Friedrich-Schiller-Universität

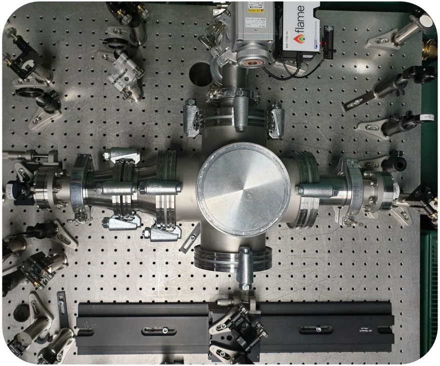

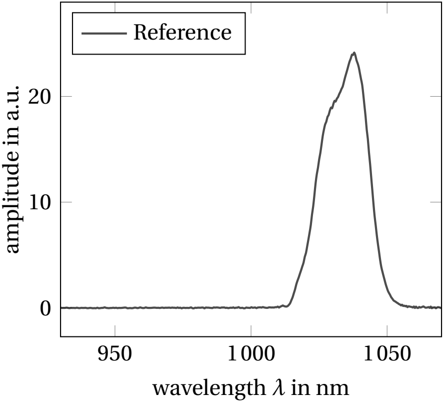

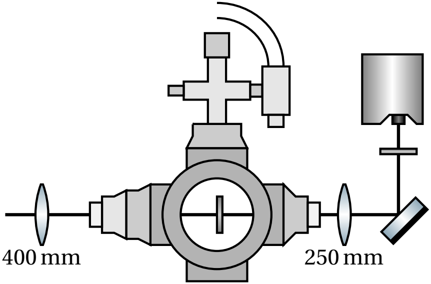
400 mm
250 mm

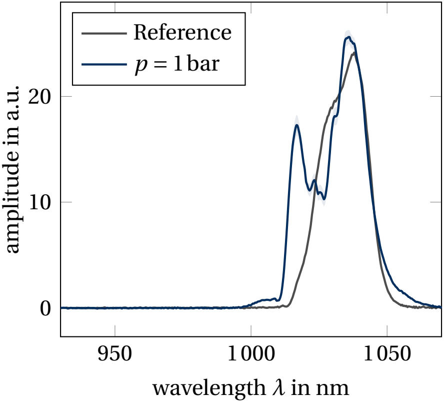
Reference
$p = 1$ bar
amplitude in a.u.
20
10
0
950
1 000
1 050
wavelength λ in nm

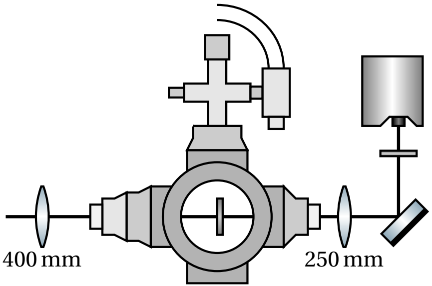
400 mm
250 mm

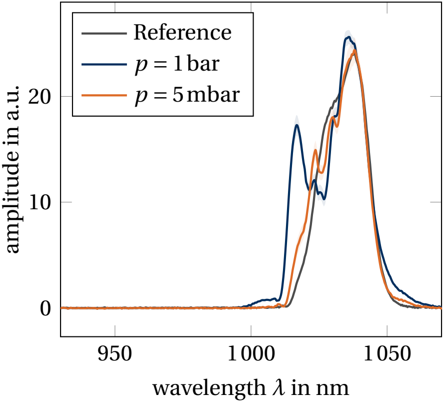
Reference
$p = 1$ bar
$p = 5$ mbar
amplitude in a.u.
20
10
0
950
1 000
1 050
wavelength λ in nm

SPM - spectral measurement in vacuum

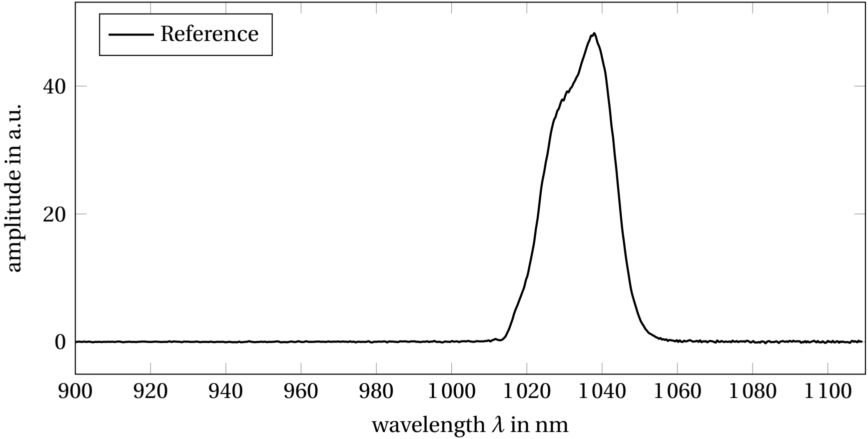

Fig.: Measurement of SPM in CR-39 performed at low pressure (5 mbar). Different pulse energies were used at a constant distance (2 cm) to the laser focus (focusing lens $f = 400$ mm).

SPM - spectral measurement in vacuum

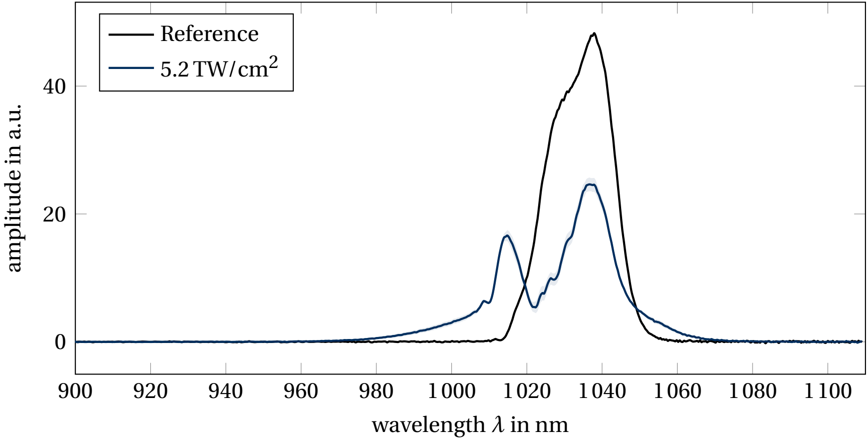

Fig.: Measurement of SPM in CR-39 performed at low pressure (5 mbar). Different pulse energies were used at a constant distance (2 cm) to the laser focus (focusing lens $f = 400$ mm).

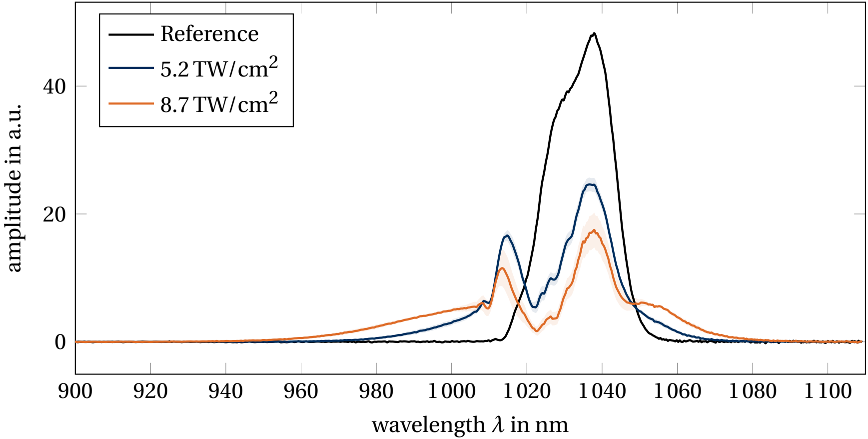

Fig.: Measurement of SPM in CR-39 performed at low pressure (5 mbar). Different pulse energies were used at a constant distance (2 cm) to the laser focus (focusing lens $f = 400$ mm).

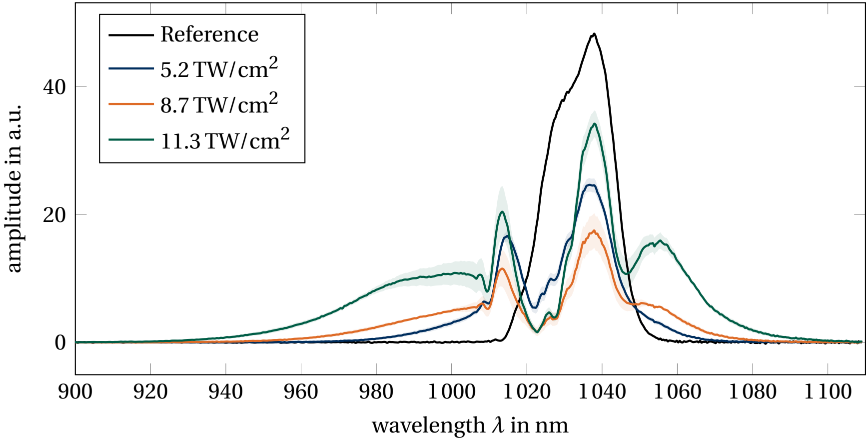

Fig.: Measurement of SPM in CR-39 performed at low pressure (5 mbar). Different pulse energies were used at a constant distance (2 cm) to the laser focus (focusing lens $f = 400$ mm).

SPM - spectral measurement in vacuum

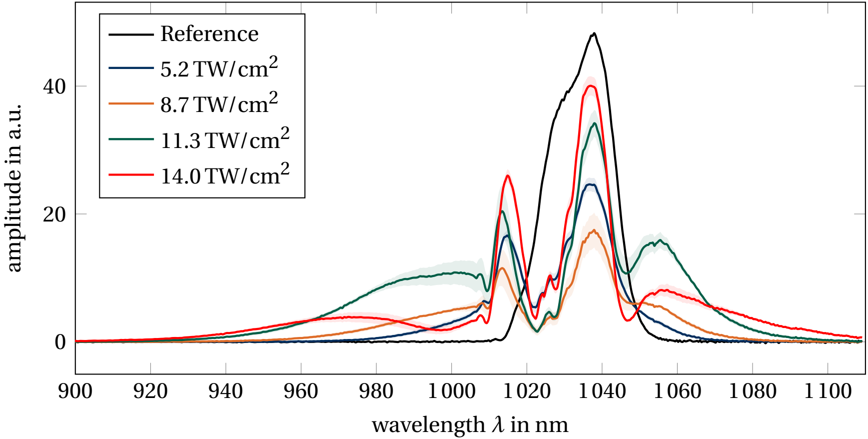

Fig.: Measurement of SPM in CR-39 performed at low pressure (5 mbar). Different pulse energies were used at a constant distance (2 cm) to the laser focus (focusing lens $f = 400$ mm).

Multi-pass cell

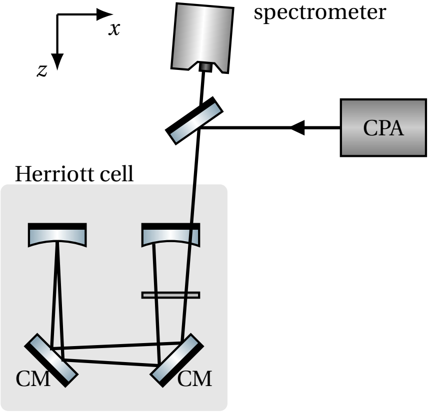

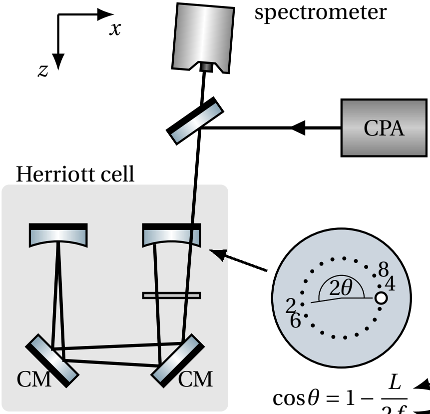

$$\cos\theta = 1 - \frac{L}{2f}$$

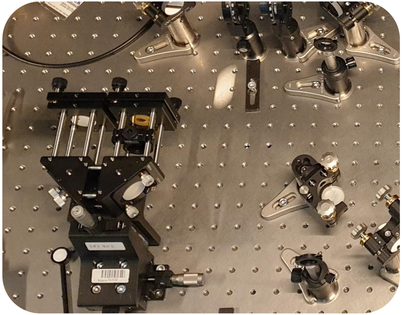

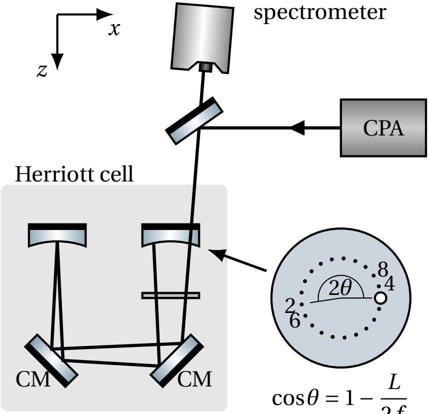

$$\cos\theta = 1 - \frac{L}{2f}$$

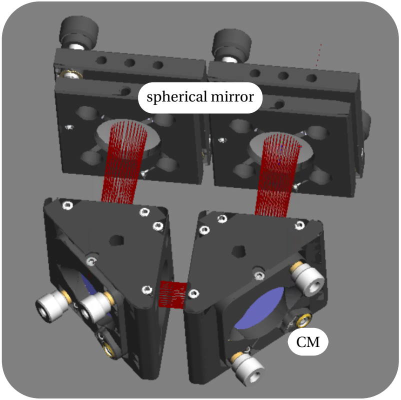

SPM - Pulse steepening

Wave equation of a plane wave in a nonlinear, inversion symmetric medium with slowly varying envelope approximation

$$\left(\frac{\partial^2}{\partial z^2} - \frac{n_0^2}{c^2}\frac{\partial^2}{\partial t^2}\right)\boldsymbol{E} = \frac{1}{c^2\varepsilon_0}\frac{\partial^2}{\partial t^2}\boldsymbol{P}^{(3)} \quad \text{with} \quad \boldsymbol{P}^{(3)} = \frac{3}{4}\varepsilon_0\chi^{(3)}|\boldsymbol{E}|^2\boldsymbol{E}.$$

Without slowly varying envelope approximation: $(\boldsymbol{E}(t) = \mathscr{E}\mathrm{e}^{\mathrm{i}(kz-\omega t)})$

$$\left(\frac{\partial}{\partial z} + \frac{n_0}{c}\frac{\partial}{\partial t}\right)\mathscr{E} + \frac{1}{2\mathrm{i}k}\left(\frac{\partial^2}{\partial z^2} - \frac{n_0^2}{c^2}\frac{\partial^2}{\partial t^2}\right)\mathscr{E} = \frac{1}{2\mathrm{i}k}\frac{3\omega_0^2}{4c^2}\left(\frac{1}{\omega_0^2}\frac{\partial^2}{\partial t^2} - \frac{2\mathrm{i}}{\omega_0}\frac{\partial}{\partial t} - 1\right)\chi^{(3)}|\mathscr{E}|^2\mathscr{E}.$$

Further simplification and splitting of amplitude $|\mathscr{E}|$ and phase Φ yields

$$\left[\frac{\partial}{\partial z} + \frac{n_0}{c}\left(1 + \frac{3\tilde{n}_2}{n_0}|\mathscr{E}|^2\right)\frac{\partial}{\partial t}\right]|\mathscr{E}| = 0,$$

$$\left[\frac{\partial}{\partial z} + \frac{n_0}{c}\left(1 + \frac{\tilde{n}_2}{n_0}|\mathscr{E}|^2\right)\frac{\partial}{\partial t}\right]\Phi = \frac{\tilde{n}_2\omega_0}{c}|\mathscr{E}|^2.$$